ACR Oct. 1942

NATIONAL ADVISORY COMMITTEE FOR AERONAUTICS

WARTIME REPORT

ORIGINALLY ISSUED
October 1942 as
Advance Confidential Report

TESTS IN THE 19-FOOT PRESSURE TUNNEL OF A 1/2.75-SCALE MODEL OF THE F4U-1 AIRPLANE WITH SEVERAL BALANCED ELEVATORS, FULL-SPAN FLAPS, AND DROPPABLE GAS TANK

By Robert R. Graham and C. Dixon Ashworth

Langley Memorial Aeronautical Laboratory
Langley Field, Va.

WASHINGTON

NATIONAL ADVISORY COMMITTEE FOR AERONAUTICS

ADVANCE CONFIDENTIAL REPORT

TESTS IN THE 19-FOOT PRESSURE TUNNEL OF A 1/2.75-SCALE MODEL OF THE F4U-1 AIRPLANE WITH SEVERAL BALANCED ELEVATORS, FULL-SPAN FLAPS, AND DROPPABLE GAS TANK

By Robert R. Graham and C. Dixon Ashworth

SUMMARY

An investigation was made in the NACA 19-foot pressure tunnel to determine the aerodynamic effects of several elevators with varying amounts of balance, of outboard split flaps, and of a droppable gas tank on a 1/2.75-scale model of the F4U-1 airplane. The investigation included:

(a) Measurements of the hinge-moment characteristics and effectiveness of various elevators;

(b) Measurements of the effects of adding split flaps outboard of the normal slotted flaps and ahead of the ailerons, on the stalling and control characteristics of the model; and

(c) Measurements of the effects of suspending a droppable gas tank below the fuselage on the lift, drag, and longitudinal stability of the model.

In order to provide a basis for comparison of the various balanced elevators, stick forces for various indicated airspeeds were computed for each elevator from the power-off results. The power-on results are not complete enough to obtain the effect of power on the elevator stick forces.

The outboard split flaps increased the maximum lift coefficient approximately 6 percent with power on and 9 percent with power off. They had a negligible effect on the stalling characteristics and the longitudinal stability but reduced the aileron effectiveness.

The droppable gas tank had no measurable effect on the maximum lift coefficient or the longitudinal stability of

the model. Its drag increment at 100 miles per hour amounted to 9 pounds and 14 pounds at lift coefficients of 0.16 and 0.5, respectively.

INTRODUCTION

During the past several years the NACA has conducted numerous investigations of a 1/2.75-scale model of the F4U-1 airplane. Much of the aerodynamic design of the full-scale airplane has been based on the results of these wind-tunnel investigations. This paper summarizes one phase of these tests.

The tests were conducted at atmospheric pressure in the NACA 19-foot pressure tunnel during the period from March 30 to April 17, 1942. They included measurements, with and without propeller operating, of the effect of several balanced elevators, of full-span flaps, and of droppable gas tank on lift, drag, and pitching moment. The hinge moments of the elevators were also determined. Aileron characteristics were measured with partial-span and full-span flaps. Tuft studies were made of the stalling characteristics with the full-span flaps.

This paper was originally issued as a memorandum report to the Bureau of Aeronautics, Navy Department.

MODEL

The 1/2.75-scale model of the F4U-1 airplane is shown in figure 1. Section views of the elevators and ailerons used on the present model are presented in figures 2 and 3. For the purpose of this investigation the model was modified as follows:

1. A remote-control apparatus for operating the elevators was installed.

2. NACA remote indicating hinge-moment balances were installed in the right aileron and in the elevator to measure the aileron and elevator hinge moments.

3. The horizontal tail of the model was arranged to allow for various modifications to the elevator.

Several elevator noses were supplied. These noses gave the elevator five arrangements involving two different hinge lines and various amounts of aerodynamic balance (fig. 2). The horn balance of elevator 5 is shown in figure 1.

4. The model was equipped with outboard split flaps (figs. 3 and 4) for use in conjunction with the inboard slotted flaps. With the slotted flaps deflected 50°, the following split-flap arrangements were tested: 0.20c flaps deflected 40° and 48°, and 0.30c flaps deflected 40°.

5. A droppable external gas tank was mounted on the bottom of the fuselage (fig. 5) for some of the tests. The shape and dimensions of the model tank are presented in figure 6.

For certain of the tests the airplane model was equipped with a propeller (see fig. 7) geometrically similar to that used on the full-scale airplane. The model propeller is 4.82 feet in diameter.

The propeller was driven by a water-cooled alternating-current induction motor capable of developing 60 horsepower at 5000 rpm. Current was supplied to the motor by a variable-frequency alternator and speed control was obtained by varying the frequency. The power output of the motor was determined from a calibration that involved current, revolution speed, and torque.

The power, cooling-water, tachometer, and hinge-moment leads were threaded behind the wing supports, through the support fairing, from the wings of the model to the test chamber below. The leads between the lower surface of the wing and the top of the support fairing were exposed to the air stream for all of the tests except the model-support tare tests. These leads are shown in figure 7.

For certain tests the horizontal tail was removed. The portion of the horizontal tail located within the fuselage was replaced with blocks that conformed to the fuselage contour (fig. 8).

The model was finished with several coats of lacquer and rubbed with No. 400 carborundum cloth in a chordwise direction until the surfaces were aerodynamically smooth.

A list of model arrangements tested is presented in table I. Changes in arrangement do not refer to changes in control-surface setting but only to changes in the contour of the model.

SYMBOLS AND COEFFICIENTS

The data in this report are reduced to standard nondimensional coefficient form. All forces and moments are given with respect to the wind axes. The coefficients and symbols involved are defined as follows:

C_L lift coefficient (L/qS)

C_D drag coefficient (D/qS)

C_{R_D} resultant-force coefficient in the drag direction (R_D/qS)

C_m pitching-moment coefficient (M/qcS)

C_l rolling-moment coefficient (L/qbS)

C_n yawing-moment coefficient (N/qbS)

C_{h_e} elevator hinge-moment coefficient ($H_e/qb_e\bar{c}_e^2$)

C_{h_a} aileron hinge-moment coefficient ($H_a/qb_a\bar{c}_a^2$)

T_c thrust disk-loading coefficient ($T/2qD^2$)

where

q dynamic pressure in the undisturbed air stream $\left(\frac{1}{2}\rho V^2\right)$

ρ mass density of air

V velocity of air

V_i indicated airspeed

L lift

D drag

R_D resultant force along wind axis (propeller operating)

M pitching moment about center of gravity of airplane

L rolling moment about center of gravity of airplane

N yawing moment about center of gravity of airplane

F_e elevator stick force, pounds ($0.45H_e$)

H_e elevator hinge moment

H_a aileron hinge moment

T effective thrust of propeller ($T-\Delta D$)

S wing area (41.6 sq ft)

c mean aerodynamic chord of wing (2.85 ft)

b wing span (14.91 ft)

$b_e\bar{c}_e^2$ product of elevator span and mean-square elevator chord (1.543 ft^3 for elevators 1, 2, and 5); (1.173 ft^3 for elevators 3 and 4)

$b_a\bar{c}_a^2$ product of aileron span and mean-square aileron chord (0.566 ft^3)

D propeller diameter (4.83 ft)

and

β propeller blade angle at 0.75 radius

α angle of attack of wing root chord line

δ_f slotted flap deflection, measured between wing chord line and flap chord line

$\delta_{f_{sp}}$ split flap deflection, measured between lower surface of wing and flap chord line

δ_e elevator deflection, measured between stabilizer chord line and elevator chord line, positive deflection with trailing edge down

δ_a aileron deflection, measured between wing chord line and aileron chord line, positive deflection with trailing edge down

δ_{a_r} right aileron deflection

δ_{a_l} left aileron deflection

i_t angle of stabilizer setting (relative to the thrust line)

R test Reynolds number based on mean aerodynamic chord ($\rho Vc/\mu$)

μ coefficient of viscosity

TEST AND RESULTS

For convenience in classifying the results and showing their location in the report, table II is presented. The tests and results are described in the following sections.

Interference corrections.- The effects of support interference and air-flow misalinement on the lift, drag, and pitching-moment characteristics were determined from tests of the model with flaps neutral and propeller removed. In order to provide proper clearance between the model and the support fairings, these tests were made without the vertical tail on the model. All results in this report have been corrected for these effects.

The angle of attack and the drag coefficient have been corrected for the effect of jet-boundary interference. Inasmuch as the results presented in this report are primarily of a comparative nature, no jet-boundary interference corrections have been applied to the pitching-moment data. These corrections may be applied by adding algebraically 0.0216 C_L for the power-off tests and 0.0258 C_L for the power-on tests. The effect of these corrections is to decrease the negative slope of the pitching-moment curves. The corrections do not apply to tests with the horizontal tail removed.

Effect of various stabilizer settings on lift, drag, and longitudinal stability.- The effect of various stabilizer settings on the lift, the drag, and the pitching-moment coefficients was determined from the results of tests made with the stabilizer set at the following angles: 4.9°, 3.95°, 1.6°, -2.3°, and -5°. For each stabilizer setting, power-on and power-off runs were made with the slotted flaps deflected 0° and 50° with the ailerons drooped 0° and 9.5°, respectively. The elevator gap was sealed smooth with cellulose tape for this part of the investigation. The results of these tests are presented in figures 9 to 20.

Two flight conditions were simulated in the power-on tests. The power-on landing approach was simulated with the slotted flaps deflected and both ailerons drooped. The thrust coefficient required for level flight at a lift coefficient of 1.85 was approximated through the range of angles of attack. The full throttle climb condition was simulated with the flaps and ailerons neutral. The thrust coefficient obtained in the climb at a lift coefficient of 0.55 was approximated through the range of angles of attack.

The power-off tests were made at a dynamic pressure of approximately 25 pounds per square foot and the power-on tests were made at a dynamic pressure of approximately 13 pounds per square foot. The propeller blades were set at 15° at 0.75 radius. The thrust coefficients obtained for the power-on tests are shown in figures 21 and 22.

Effect of various elevator balances on lift, drag, pitching-moment, and elevator hinge-moment coefficients and on stick forces.- Five elevator arrangements were tested to determine their effects on lift, drag, pitching-moment, and elevator hinge-moment coefficients. Elevators with noses 1, 2, 3, and 4 (fig. 2) were tested with power-off and slotted flaps at 0°. The elevator with nose 5 is similar to the elevator now in use on the F4U-1 airplane. It was tested with power on and off and with slotted flap deflections of 0° and 50°.

For each elevator arrangement, elevator deflections of 20°, 10°, -10°, -20°, and -30° were investigated. At each elevator deflection the model was tested through a complete angle-of-attack range from below zero lift to beyond the stall. The angle of stabilizer setting was 1.5°. For those tests in which the flaps were deflected 50°, the ailerons were drooped 9.5°.

The power-off runs were made at a dynamic pressure of approximately 25 pounds per square foot. The power-on runs simulated landing approach and climbing conditions of the airplane and were made at a dynamic pressure of approximately 13 pounds per square foot.

The effects of the various elevators on the lift and drag characteristics of the model are presented in figures 23 to 30. The effects of the elevators on the pitching-moment characteristics are presented in figures 31 to 34. The hinge-moment characteristics of the various elevators are presented in figures 35 to 42.

Figure 43 shows a comparison of the stick forces and the corresponding elevator deflections for the five elevator noses for the model condition of propeller off and flaps neutral. Stick forces and elevator deflections for the elevator with nose 5 and the model condition of propeller off and flaps deflected are also shown. This figure was prepared by obtaining, from figures 23 to 42, the elevator deflections, elevator hinge-moment coefficients, and lift coefficients for zero pitching moment at several angles of attack. The lift coefficients were converted to indicated airspeed by assuming an airplane weight of 10,000 pounds. The hinge-moment coefficients were converted to full-scale hinge moments at the indicated airspeeds obtained from the corresponding lift coefficients. The stick forces were then computed from the assumed relationship, $F_e = 0.45 H_e$. For the flap-neutral condition, the stick forces were trimmed at 260 miles per hour indicated airspeed by correcting the hinge-moment coefficients an amount equal to the coefficient at that airspeed. In the same manner, the stick forces for the flap-deflected condition were trimmed at 100 miles per hour indicated airspeed.

All of these stick forces were computed with the center of gravity of the airplane located as shown in figure 1. No allowances were made for any Reynolds number effects on pitching-moment, lift, or hinge-moment coefficients.

Figure 43 shows that the stick forces for elevators with noses 1, 2, 3, and 4 are considerably less than with nose 5 for the propeller-off, flap-neutral condition.

The effect upon the drag coefficient of sealing the gap between the stabilizer and elevator is shown in figure 44.

split flap arrangements. For the first group of runs the slotted flaps were deflected 50°, the 0.20c outboard split flaps 48°, and the left aileron 0°. Tests were then made without the outboard split flaps, with the slotted flaps deflected 50°, and the left aileron set at 9.5°. Further investigation was carried out with a slotted flap deflection of 30°, with the split flaps removed, and with the left aileron set at 7.85°.

All these tests were made at a dynamic pressure of approximately 25 pounds per square foot with the stabilizer set at 1.6°. The right aileron (fig. 3) was set at the following angles: 20°, 10°, 0°, −10°, −15°, and −20°. For each aileron setting the model was tested at approximately 0°, 6°, and 12° angle of attack.

The results of these tests are presented in figures 50 to 57.

A comparison of figure 51 with 53 shows that the effectiveness of the ailerons is considerably reduced by the installation of the outboard split flaps.

Effect of droppable external gas tank on lift, drag, and pitching-moment coefficients.— Tests were made with the droppable gas tank shown in figure 6 located on the model as shown in figure 5. Two runs were made: one with the slotted flaps and ailerons at 0°, and the other with the slotted flaps deflected 50° and the ailerons drooped 9.5°. The model was tested through an angle-of-attack range from below zero lift to beyond the stall. The results of these tests are shown in figures 58 and 59.

From figure 58 it will be noted that the droppable gas tank had no effect on the maximum lift coefficient of the model. The tank also had no aerodynamic effect on the power-off longitudinal stability of the model. From figure 59, it is seen that the droppable gas tank increases the drag coefficient of the model 0.0011 at the high speed C_L of 0.16, and 0.0017 at a C_L of 0.55. These drag increments amount to a drag, at 100 miles per hour, of 9 and 14 pounds, respectively.

Effect of outboard split flaps on the stalling characteristics of the wing.— A study of the stalling characteristics of the wing for several arrangements of the model was made by observing the behavior of wool tufts on the model.

Effect of removing the horizontal tail on lift, drag, and longitudinal stability.- The horizontal tail was removed and that portion of the horizontal tail located within the fuselage was replaced with blocks that conformed to the fuselage contour. This arrangement is shown in figure 8. Runs were made with the slotted flaps set at 0° and 50° and with the ailerons drooped 0° and 9.5°, respectively. Power-on and power-off runs were made for each flap and aileron setting.

The power-on and power-off runs were made at dynamic pressures of 13 and 25 pounds per square foot, respectively; the power-on runs simulated the same airplane flight conditions as in the stabilizer and elevator tests. The results of these tests are presented in figures 45 and 46.

Effect of full-span flaps on lift, drag, and pitching-moment coefficients.- Tests were made with the slotted flaps at 50° and with various arrangements of outboard split flaps. At a dynamic pressure of approximately 25 pounds per square foot, runs were made with 0.20c split flaps at 40° (fig. 4) and 48° and with 0.30c split flaps at 40°. Further investigation was made with power on and power off at a dynamic pressure of 8.4 pounds per square foot for the 0.20c and 0.30c split flaps at 40°. The power-on runs were made at a dynamic pressure of 8.4 pounds per square foot with the propeller blade angle set 20° at 0.75 radius. The angle of the stabilizer was 1.6°.

The power-on condition of the model simulated power-on landing-approach condition of the F4U-1 airplane. The results of these tests are given in figures 47 to 49.

Figures 47 to 49 show that the optimum of the three conditions of outboard split flap tested is the 0.30c flap deflected 40°. With this outboard split flap condition, the slotted flaps deflected 50°, and the ailerons neutral, a maximum lift coefficient of 2.32 was obtained with power off and 2.61 with power on as compared with 2.13 and 2.46 with the split flaps off, the slotted flaps deflected 50°, and the ailerons drooped 9.5°. The effect of the outboard split flaps on the pitching-moment coefficient curve is to slightly increase its negative slope in the angle-of-attack range just below the stall.

Effect of various flap arrangements on aileron characteristics.- Three groups of tests were made to determine the effect on aileron characteristics of various outboard

no measurable effect on the maximum lift and no measurable aerodynamic effect on the power-off longitudinal stability.

Langley Memorial Aeronautical Laboratory,
National Advisory Committee for Aeronautics,
Langley Field, Va.

Tufts were attached to the upper surface of the wing and flaps with cellulose tape at 20-, 30-, 40-, 50-, 60-, 70-, 80-, and 90-percent-chord stations. The tufts were spaced about 7 inches in a spanwise direction. The progression of the stall with increase in angle of attack was recorded by sketching the stalled portions of the wing at various angles of attack. Force measurements were taken during each of the stall-observation tests.

For this series of tests only the effect of the addition of outboard split flaps on the stalling characteristics of the wing was desired. The investigation was made with the slotted flaps deflected 50° and with the 0.30c outboard split flaps deflected 40°. All other control surfaces were set at 0°; the stabilizer was set at 1.6°.

The power-on stall test was made to simulate a powered-landing-approach condition of the airplane. Power-on and power-off tests were made at dynamic pressures of 8.4 pounds per square foot and 25 pounds per square foot, respectively. The results of these tests are presented in figures 60 and 61.

A comparison of figures 60 and 61 with unpublished data shows that with the slotted flaps deflected the stalling characteristics are approximately the same for the two conditions of outboard split flaps deflected 40° and ailerons 0°, and outboard split flaps 0° and ailerons drooped 9.5°.

CONCLUSIONS

1. The maximum lift coefficient for the power-on landing approach was 6 percent higher with both inboard slotted flaps and outboard split flaps deflected than it was with inboard slotted flaps deflected and ailerons drooped.

2. The addition of the outboard split flaps had a negligible effect on the stalling characteristics and the longitudinal stability but noticeably reduced the aileron effectiveness.

3. The droppable gas tank caused drag increments at 100 miles per hour amounting to 9 pounds and 14 pounds at lift coefficients of 0.16 and 0.55, respectively. It had

TABLE I

F4U-1 MODEL ARRANGEMENTS FOR 19-FOOT PRESSURE TUNNEL TESTS

Model arrangements	Vertical tail on	Horizontal tail on	Propeller on β 15°	Propeller on β 20°	Elevator noses on 1	2	3	4	5	Elevator plastered smooth	Outboard split flaps on	Tufts on	Droppable gas tank on
B	X	X							X	X			
C	X	X	X						X	X			
D	X	X	X						X				
E	X	X							X				
F	X	X			X								
G	X	X				X							
H	X	X					X						
I	X	X						X					
J	X												
K	X		X										
L	X	X							X		X		
M	X	X		X					X		X		
N	X	X		X					X		X	X	
O	X	X							X		X	X	
P	X	X							X				X

Figure	Type of test	Model arrangements	i_t (deg)	δ_f (deg)	0.20c $\delta_{f_{sp}}$ (deg)	0.30c $\delta_{f_{sp}}$ (deg)	δ_{a_r} (deg)	δ_{a_l} (deg)	δ_e (deg)	Values of angle of attack, α (deg)
9	C_L and C_D against α	B	4.9	$\frac{0}{50}$	off	off	$\frac{0}{9.5}$	$\frac{0}{9.5}$	0	
10	C_L and C_{R_D} against α	C	4.9	$\frac{0}{50}$	-do-	-do-	$\frac{0}{9.5}$	$\frac{0}{9.5}$	0	
11	C_L and C_D against α	B	3.95	$\frac{0}{50}$	-do-	-do-	$\frac{0}{9.5}$	$\frac{0}{9.5}$	0	
12	C_L and C_{R_D} against α	C	3.95	$\frac{0}{50}$	-do-	-do-	$\frac{0}{9.5}$	$\frac{0}{9.5}$	0	
13	C_L and C_D against α	B	1.6	$\frac{0}{50}$	-do-	-do-	$\frac{0}{9.5}$	$\frac{0}{9.5}$	0	
14	C_L and C_{R_D} against α	C	1.6	$\frac{0}{50}$	-do-	-do-	$\frac{0}{9.5}$	$\frac{0}{9.5}$	0	
15	C_L and C_D against α	B	-2.3	$\frac{0}{50}$	-do-	-do-	$\frac{0}{9.5}$	$\frac{0}{9.5}$	0	
16	C_L and C_{R_D} against α	C	-2.3	$\frac{0}{50}$	-do-	-do-	$\frac{0}{9.5}$	$\frac{0}{9.5}$	0	
17	C_L and C_D against α	B	-5.0	$\frac{0}{50}$	-do-	-do-	$\frac{0}{9.5}$	$\frac{0}{9.5}$	0	
18	C_L and C_{R_D} against α	C	-5.0	$\frac{0}{50}$	-do-	-do-	$\frac{0}{9.5}$	$\frac{0}{9.5}$	0	
19	C_m against α	B	range	$\frac{0}{50}$	-do-	-do-	$\frac{0}{9.5}$	$\frac{0}{9.5}$	0	
20	C_m against α	C	range	$\frac{0}{50}$	-do-	-do-	$\frac{0}{9.5}$	$\frac{0}{9.5}$	0	
21	T_c against α	C	range	0	-do-	-do-	0	0	0	
22	T_c against α	C	range	50	-do-	-do-	9.5	9.5	0	
23	C_L and C_D against α	E	1.5	50	-do-	-do-	9.5	9.5	-30 to 20	
24	C_L and C_{R_D} against α	D	1.5	50	-do-	-do-	9.5	9.5	-30 to 20	
25	C_L and C_D against α	E	1.5	0	-do-	-do-	0	0	-30 to 20	
26	C_L and C_{R_D} against α	D	1.5	0	-do-	-do-	0	0	-30 to 20	
27	C_L and C_D against α	F	1.5	0	-do-	-do-	0	0	-30 to 20	
28	C_L and C_D against α	G	1.5	0	-do-	-do-	0	0	-30 to 20	
29	C_L and C_D against α	H	1.5	0	-do-	-do-	0	0	-20 to 20	
30	C_L and C_D against α	I	1.5	0	-do-	-do-	0	0	-20 to 20	
31	C_m against α	E	1.5	$\frac{0}{50}$	-do-	-do-	$\frac{0}{9.5}$	$\frac{0}{9.5}$	-30 to 20	
32	C_m against α	D	1.5	$\frac{0}{50}$	-do-	-do-	$\frac{0}{9.5}$	$\frac{0}{9.5}$	-30 to 20	
33	C_m against α	F and G	1.5	0	-do-	-do-	0	0	-30 to 20	
34	C_m against α	H and I	1.5	0	-do-	-do-	0	0	-20 to 20	
35	C_{h_e} against α	E	1.5	50	-do-	-do-	9.5	9.5	-30 to 20	
36	C_{h_e} against α	D	1.5	50	-do-	-do-	9.5	9.5	-30 to 20	
37	C_{h_e} against α	E	1.5	0	-do-	-do-	0	0	-30 to 20	
38	C_{h_e} against α	D	1.5	0	-do-	-do-	0	0	-30 to 20	
39	C_{h_e} against α	F	1.5	0	-do-	-do-	0	0	-30 to 20	
40	C_{h_e} against α	G	1.5	0	-do-	-do-	0	0	-30 to 20	
41	C_{h_e} against α	H	1.5	0	-do-	-do-	0	0	-20 to 20	
42	C_{h_e} against α	I	1.5	0	-do-	-do-	0	0	-20 to 20	

Figure	Type of test	Model arrangements	i_t (deg)	δ_f (deg)	0.20c $\delta_{f_{sp}}$ (deg)	0.30c $\delta_{f_{sp}}$ (deg)	δ_{a_r} (deg)	δ_{a_l} (deg)	δ_e (deg)	Values of angle of attack, α (deg)
43	F_e and δ_e against V_i	E	1.5	0 50	off	off	0 9.5	0 9.5		
		F	1.5	0	-do-	-do-	0	0		
		G	1.5	0	-do-	-do-	0	0		
		H	1.5	0	-do-	-do-	0	0		
		I	1.5	0	-do-	-do-	0	0		
44	C_L against C_D	B and E	(a)	0	-do-	-do-	0	0	0	
45	C_L, C_D, and C_m against α	J	off	0 50	-do-	-do-	0 9.5	0 9.5	0	
46	C_L, C_{R_D}, and C_m against α	K	-do-	0 50	-do-	-do-	0 9.5	0 9.5	0	
47	C_L, C_D, and C_m against α	L	1.6	50	40	40	0	0	0	
48		M	1.6	50	40	40	0	0	0	
49		L	1.6	50	40 48	40	0	0	0	
50	C_L and C_D against δ_{a_r}	L	1.6	50	48	off	-20 to 20	0	0	1.2, 7.8, 14.3
51	C_l and C_n against δ_{a_r}	L	1.6	50	48	-do-	-20 to 20	0	0	1.2, 7.8, 14.3
52	C_L and C_D against δ_{a_r}	E	1.6	50	off	-do-	-20 to 20	9.5	0	0.9, 7.5, 14.1
53	C_l and C_n against δ_{a_r}	E	1.6	50	-do-	-do-	-20 to 20	9.5	0	0.9, 7.5, 14.1
54	C_L and C_D against δ_{a_r}	E	1.6	30	-do-	-do-	-20 to 20	7.85	0	0.7, 7.3, 13.9
55	C_l and C_n against δ_{a_r}	E	1.6	30	-do-	-do-	-20 to 20	7.85	0	0.7, 7.3, 13.9
56	C_m against δ_{a_r}	E	1.6	30	-do-	-do-	-20 to 20	7.85	0	0.7, 7.3, 13.9
		E	1.6	50	-do-	-do-	-20 to 20	9.5	0	0.9, 7.5, 14.1
		L	1.6	50	48	-do-	-20 to 20	0	0	1.2, 7.8, 14.3
57	Ch_a against δ_{a_r}	E	1.6	30	off	-do-	-20 to 20	7.85	0	0.7, 7.3, 13.9
		E	1.6	50	-do-	-do-	-20 to 20	9.5	0	0.9, 7.5, 14.1
		L	1.6	50	48	-do-	-20 to 20	0	0	1.2, 7.8, 14.3
58	C_L, C_D, and C_m against α	P	1.6	0 50	off	-do-	0 9.5	0 9.5	0	
59	C_L against C_D	E and P	(a)	0	-do-	-do-	0	0	0	
60	Stall diagrams	N	1.6	50	-do-	40	0	0	0	
61		O	1.6	50	-do-	40	0	0	0	

[a] i_t values are 1.5 and 1.6.

L-440

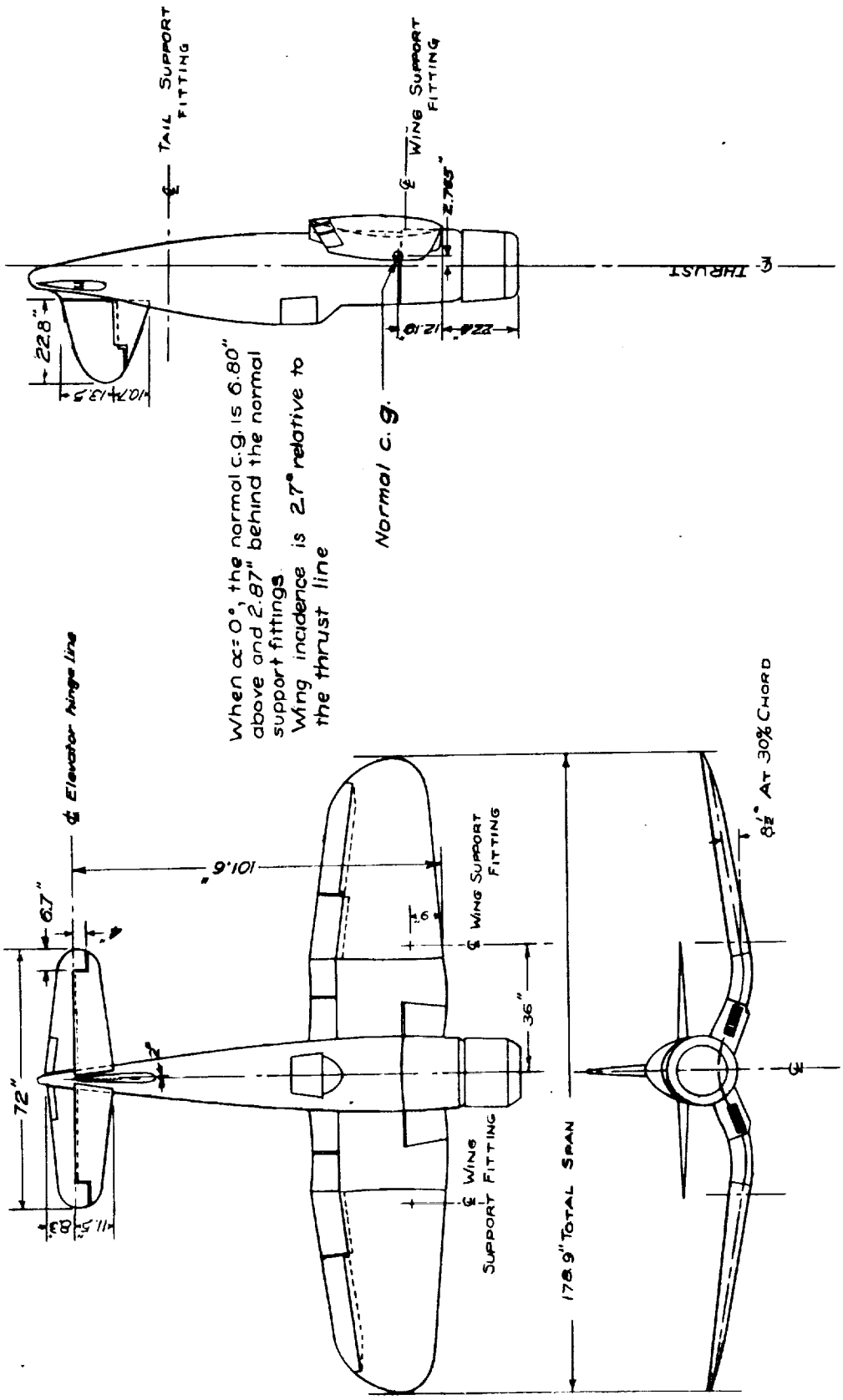

Figure 1.-Plan and elevations of $\frac{1}{2.75}$-scale model F4U-1 airplane.

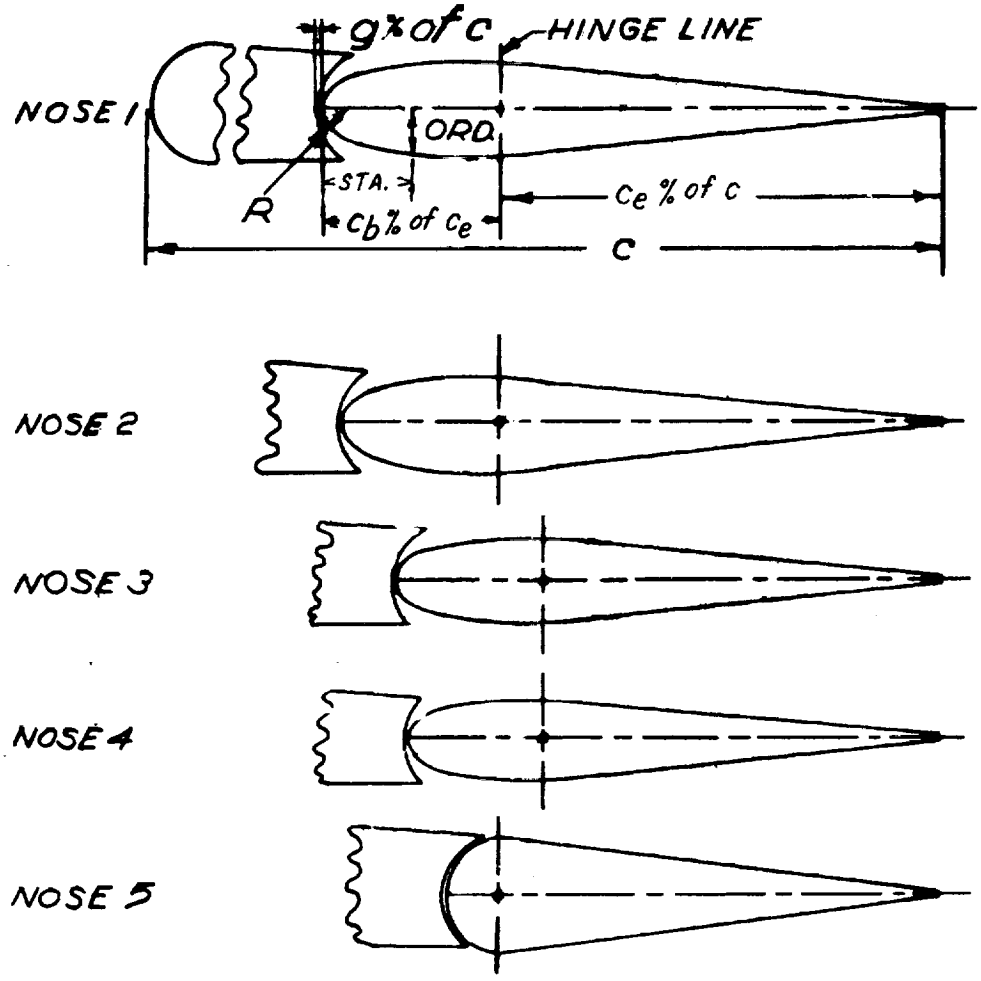

		STA	0	5%	10%	15%	20%	25%	30%	35%	40%	50%	60%	70%	80%	90%	100%	R
SECTION A-A ORDINATES	.40c ELEV	NOSE 1	0	5.38	6.72	7.61	7.98	7.82	7.56	6.94	6.52	5.47	4.36	3.36	2.35	1.51	.410	4.74
		NOSE 2	0	5.4	7.06	7.86	8.01	7.96	7.58	7.06	6.71	5.58	4.44	3.48	2.60	1.65	.427	4.36
	.35c ELEV	NOSE 3	0	5.29	6.73	7.41	7.79	7.93	7.50	6.98	6.54	5.54	4.57	3.46	2.40	1.44	.470	4.81
		NOSE 4	0	5.23	6.52	7.46	7.86	7.82	7.46	7.07	6.62	5.48	4.75	3.58	2.69	1.59	.488	4.36
	.40c	NOSES															5.92	11.15

NOSE	1	2	3	4	5
c	18.84	18.84	18.84	18.84	18.84
c_e% of c	44.4	44.4	39.6	39.6	44.4
c_b% of c_e	41.1	35.8	38.6	34.7	11.9
g% of c	.331	.331	.331	.331	.331

Figure 2.- Details of the various elevator noses taken at the theoretical intersection of the elevator and the center line of the $\frac{1}{2.75}$-scale model of the F4U-1 airplane.

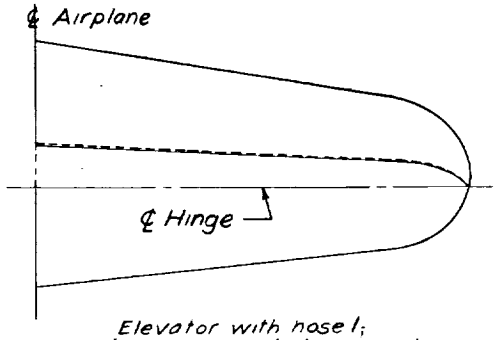

Elevator with nose 1;
balance, 41.1% elevator chord;
elevator, 40% of horizontal tail

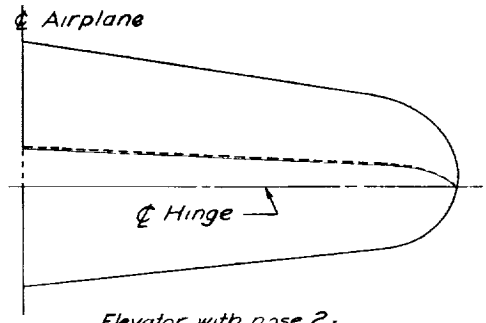

Elevator with nose 2;
balance, 35.8 % elevator chord;
elevator, 40% of horizontal tail

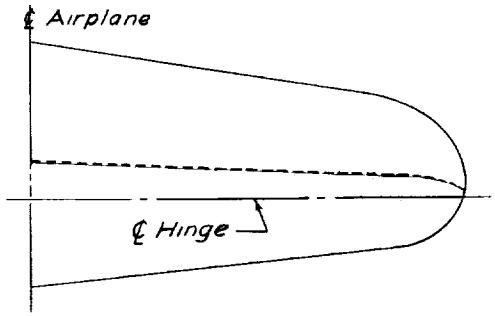

Elevator with nose 3;
balance, 38.6% elevator chord;
elevator, 35% of horizontal tail

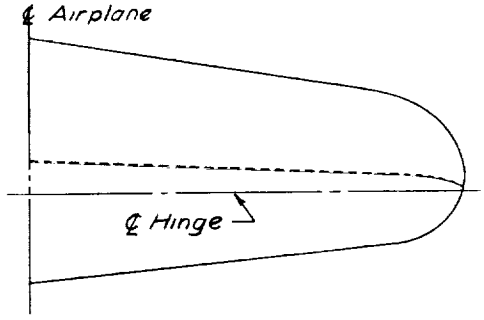

Elevator with nose 4;
balance, 34.7% elevator chord;
elevator, 35% of horizontal tail

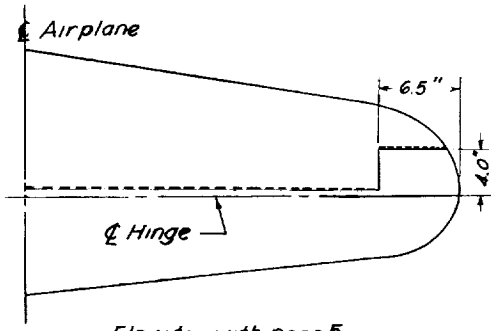

Elevator with nose 5;
balance, 11.9 % elevator chord,
with additional horn balance;
elevator, 40% of horizontal tail

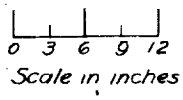

All balances are of the
constant-percent-chord type.

Figure 2(a).- Plan views of the various elevator arrangements tested on the 1/2.75-scale model of the F4U-1 airplane.

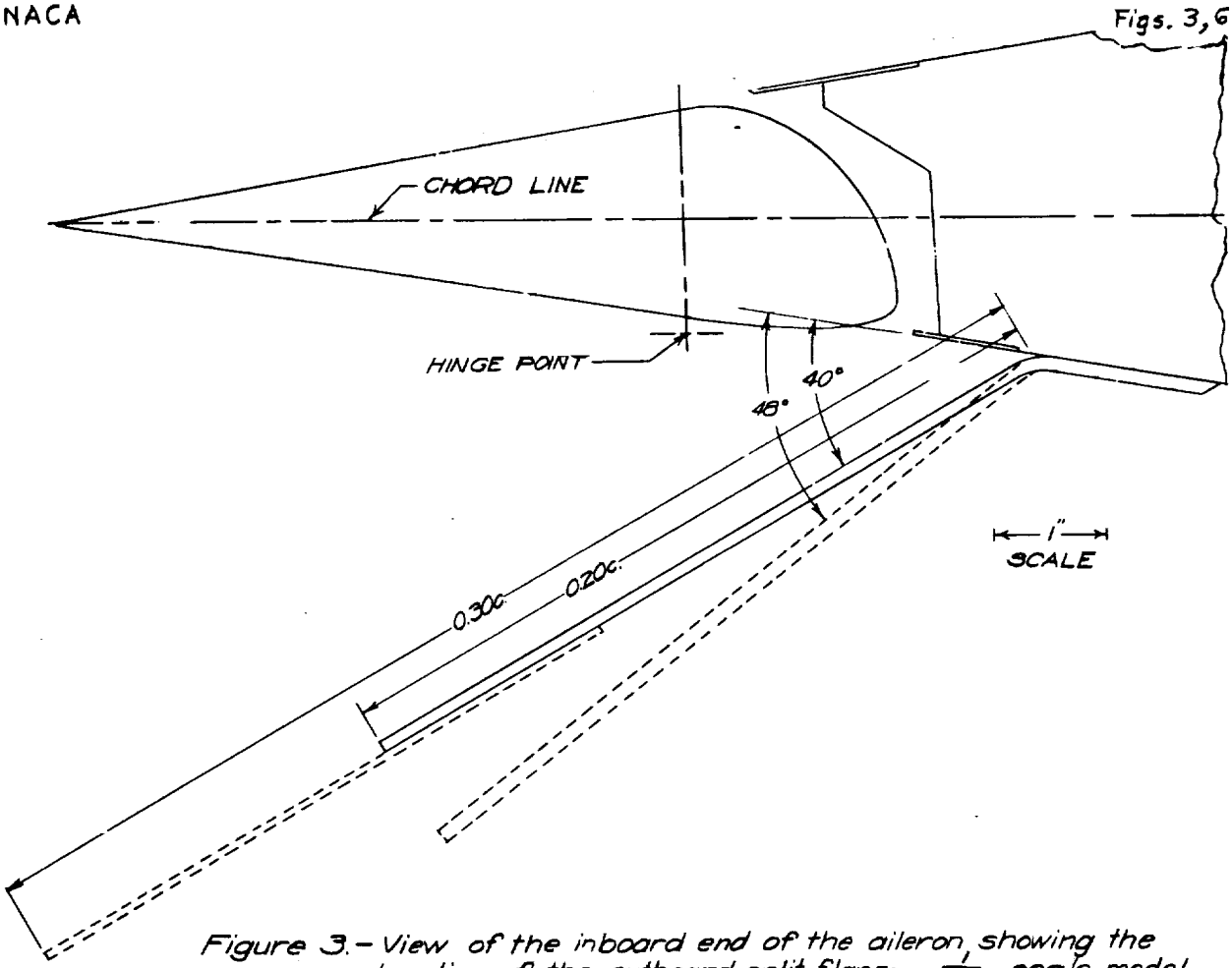

Figure 3.- View of the inboard end of the aileron, showing the location of the outboard split flaps; $\frac{1}{2.75}$-scale model of the F4U-1 airplane.

S.H.S. 9-9-43

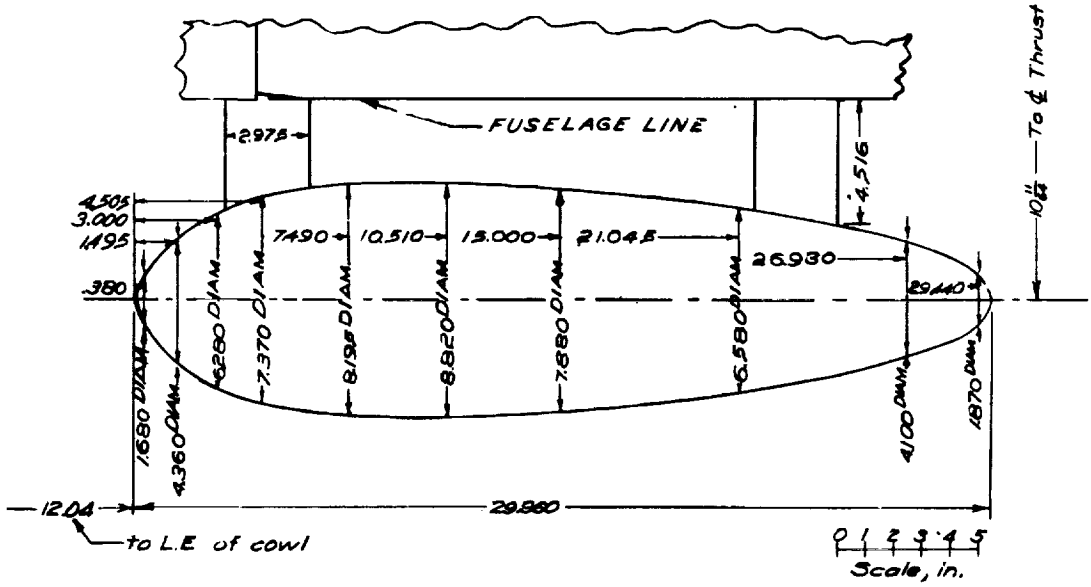

Figure 6.-Shape of droppable gas tank as used in tests of the $\frac{1}{2.75}$-scale model of the F4U-1 airplane.

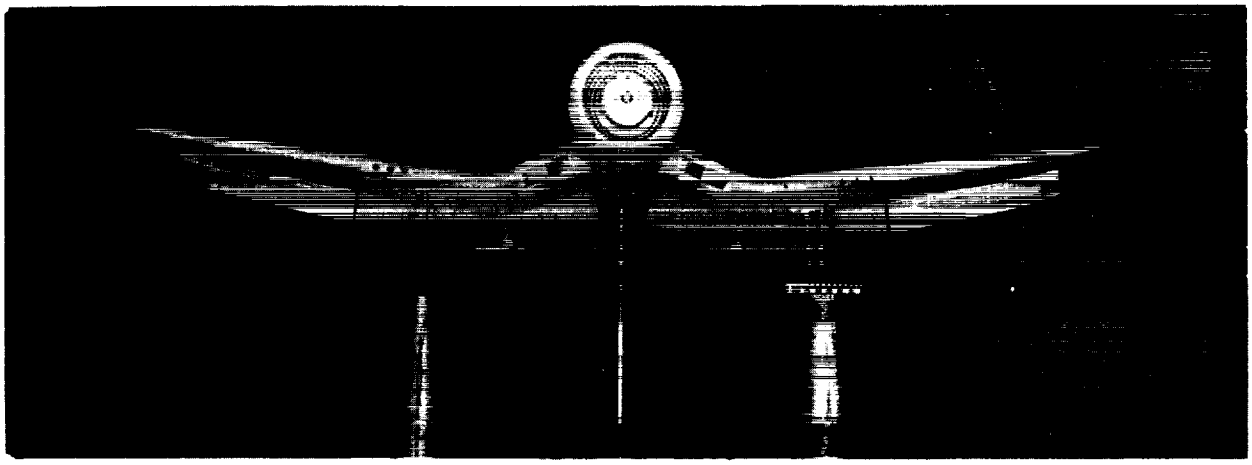

Figure 4.- The 1/2.75 scale model of the F4U-1 airplane in the 19-foot pressure tunnel showing the full-span flaps.

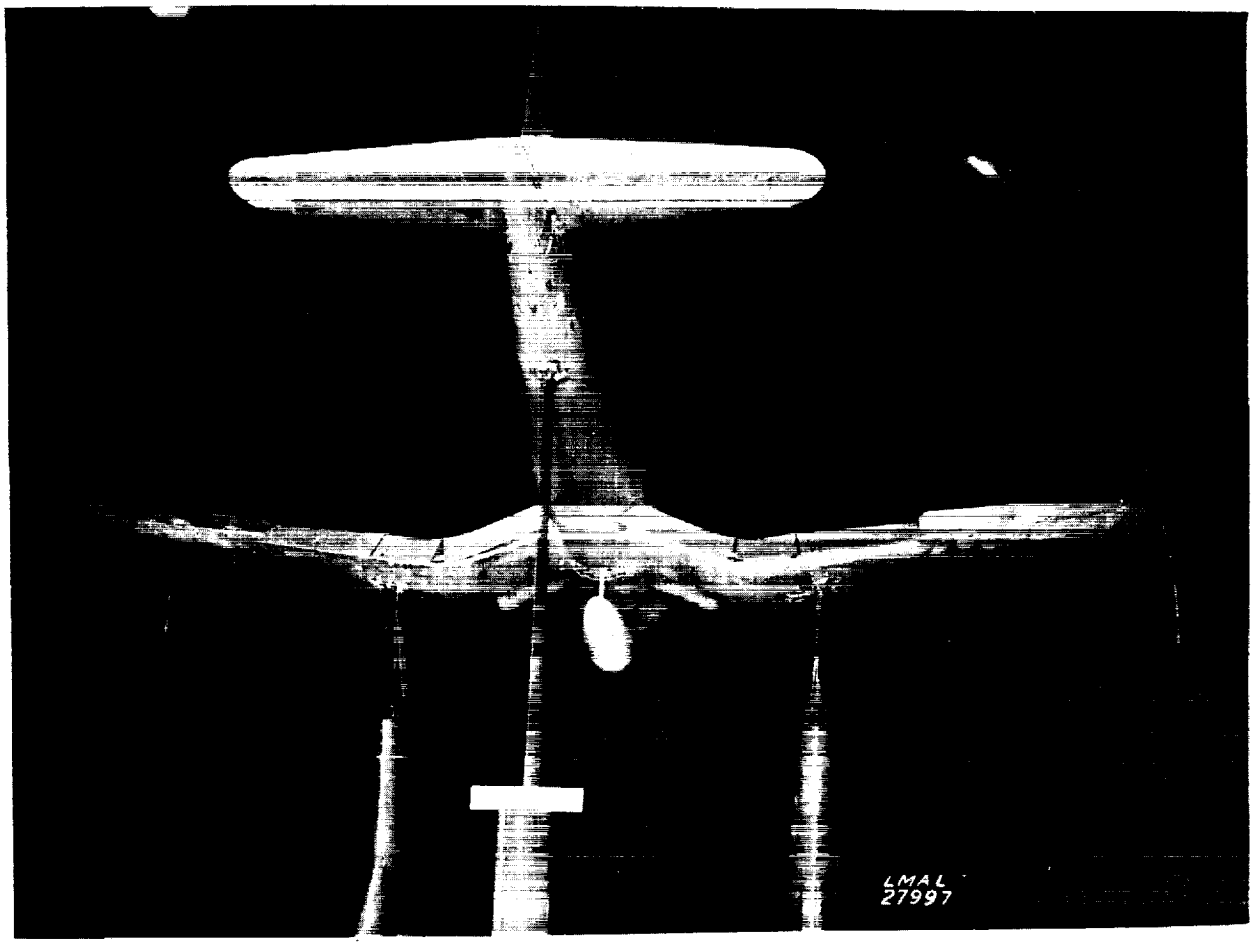

Figure 5.- Rear view of 1/2.75 scale model of the F4U-1 airplane showing the droppable external gas tank.

L-440

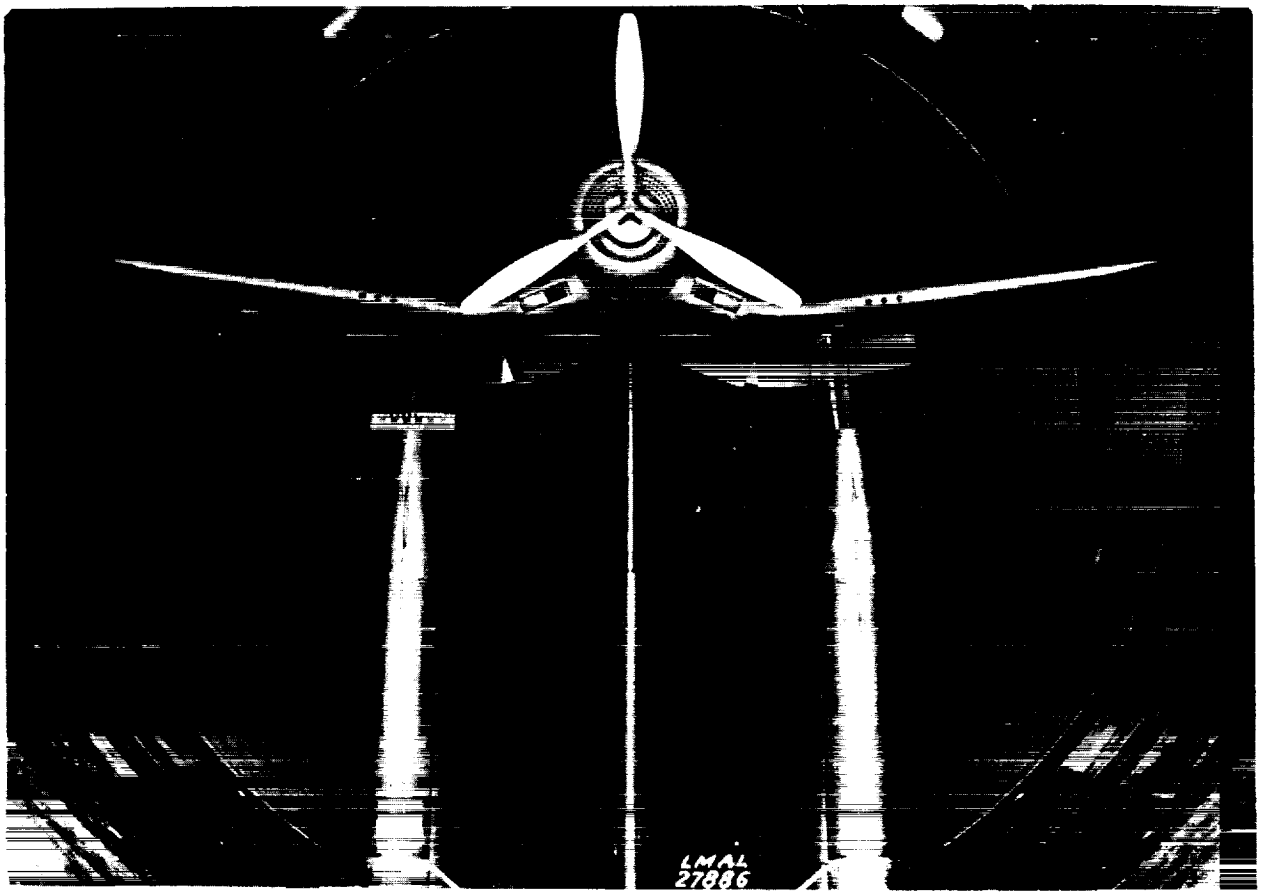

Figure 7.- The 1/2.75 scale model of the F4U-1 airplane showing propeller and slotted flaps deflected 50°.

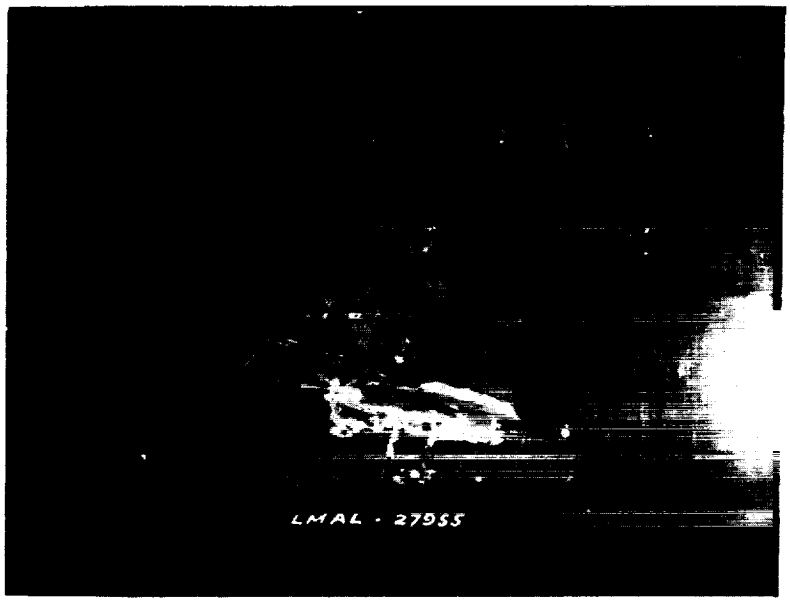

Figure 8.- View showing the 1/2.75 scale model of the F4U-1 airplane without the horizontal tail.

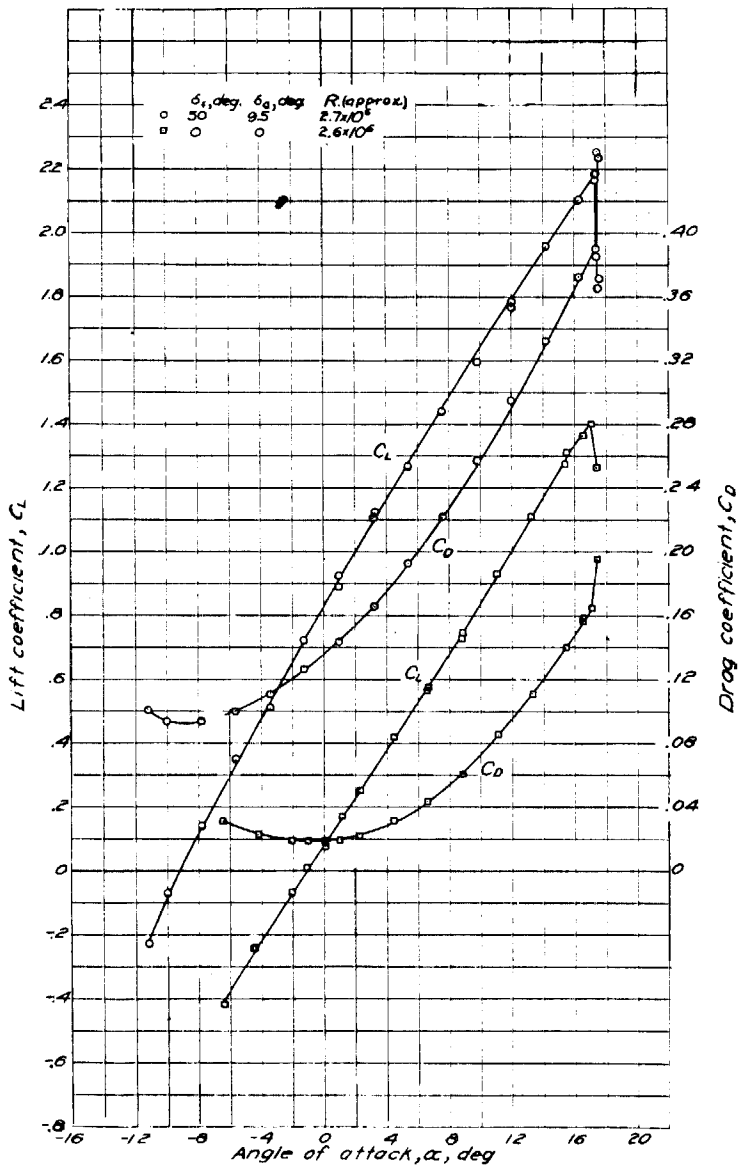

Figure 9 .-Variation of lift and drag coefficients with angle of attack; power off; $i_t = 4.9°$; $q \approx 25$ lb/sq ft.

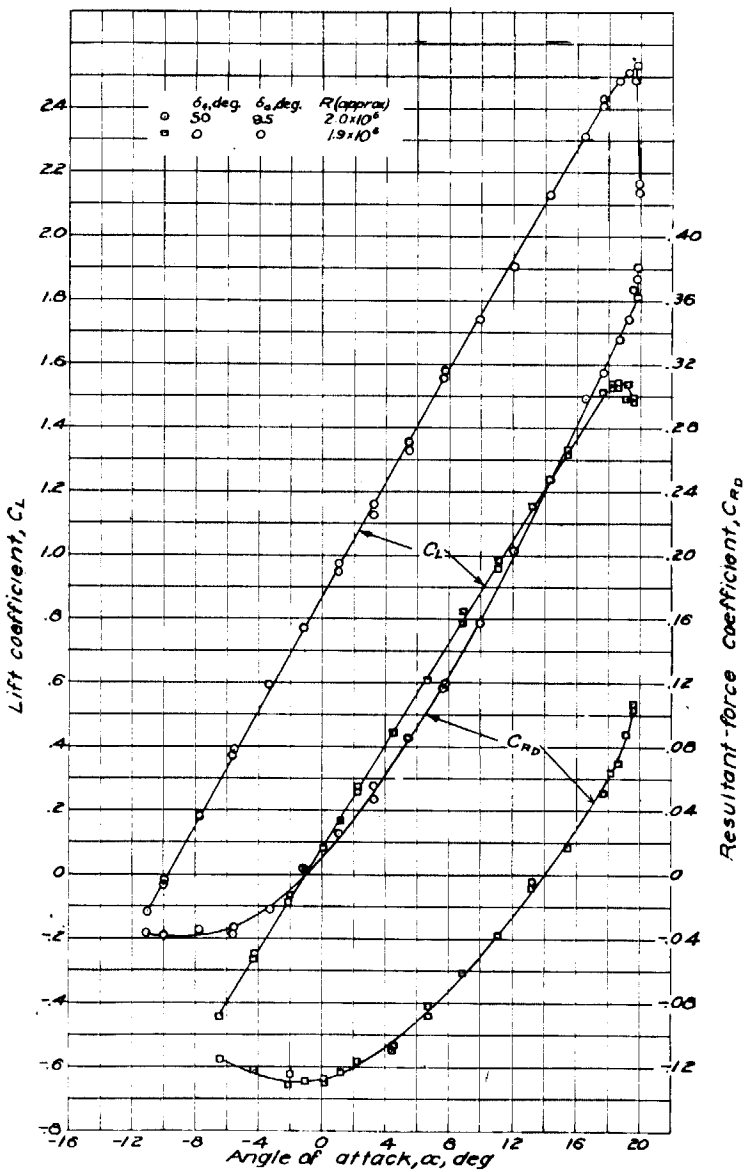

Figure 10 .-Variation of lift and resultant-force coefficients with angle of attack; power on; $i_t = 4.9°$; $q \approx 31$ lb/sq ft.

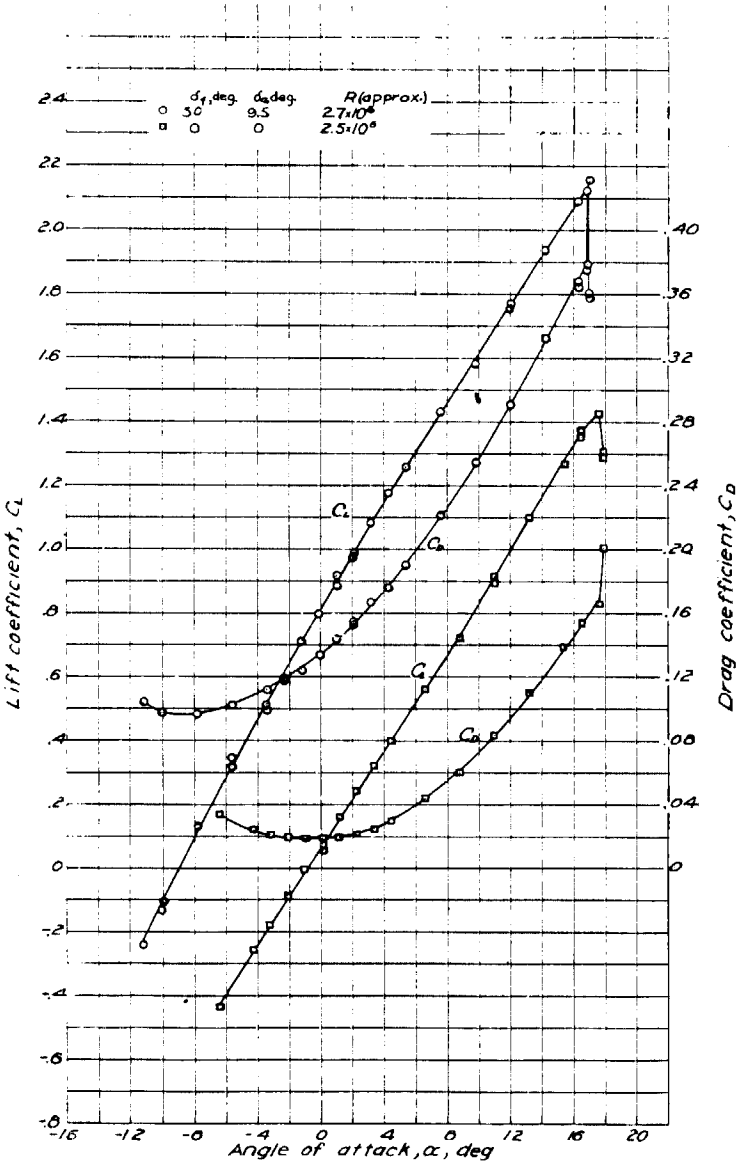

Figure 11 .-Variation of lift and drag coefficients with angle of attack; power off; i_t=3.95°; q≈25 lb/sq ft.

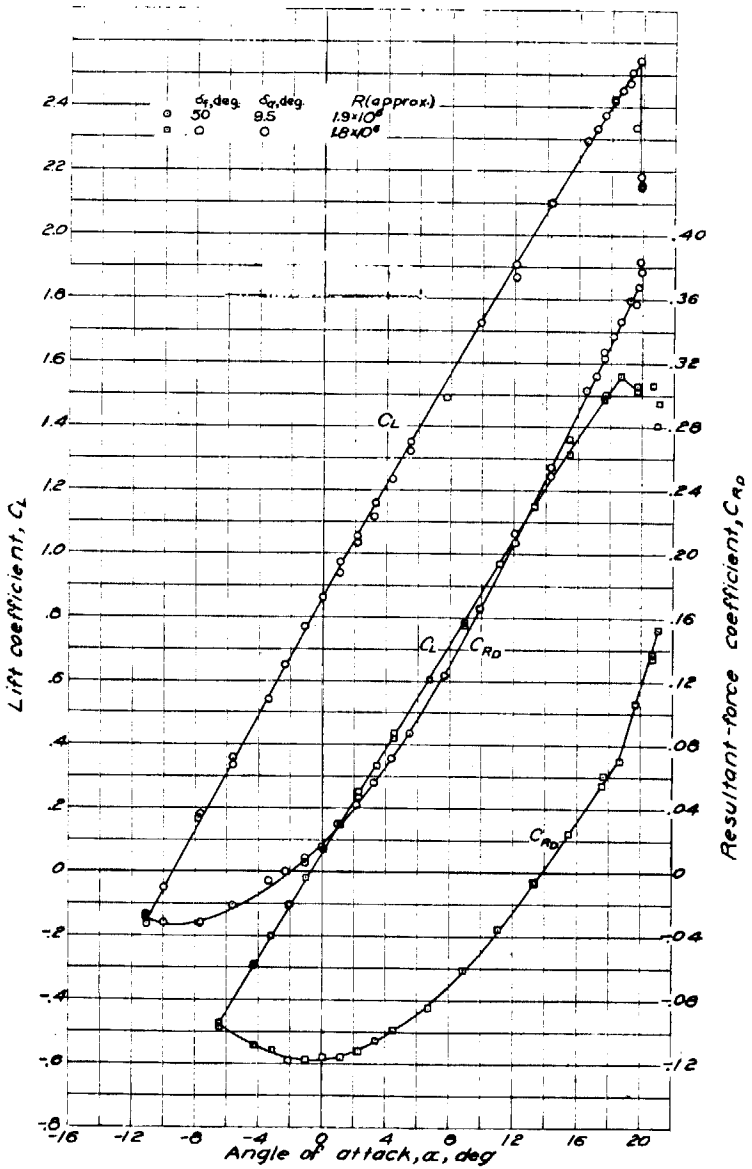

Figure 12 .-Variation of lift and resultant-force coefficients with angle of attack; power on; i_t=3.95°; q≈13 lb/sq ft.

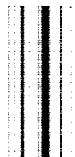

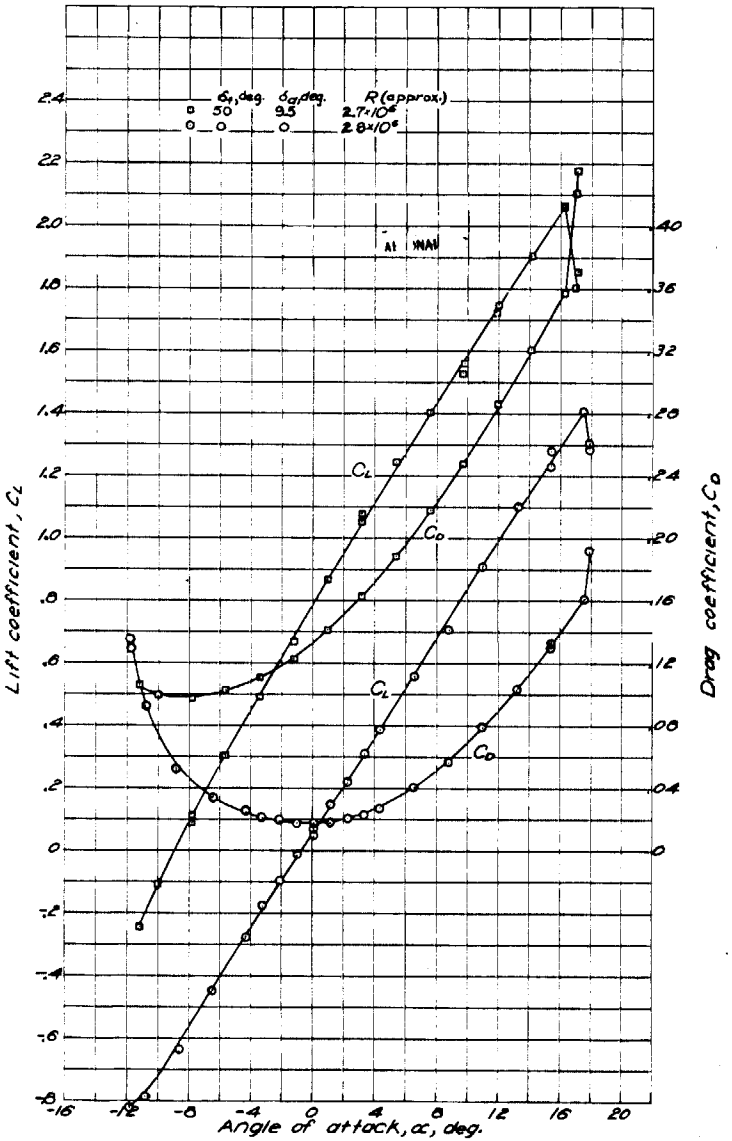

Figure 13 .-Variation of lift and drag coefficients with angle of attack; power off; i_t = 1.6°; q≈25 lb/sq ft.

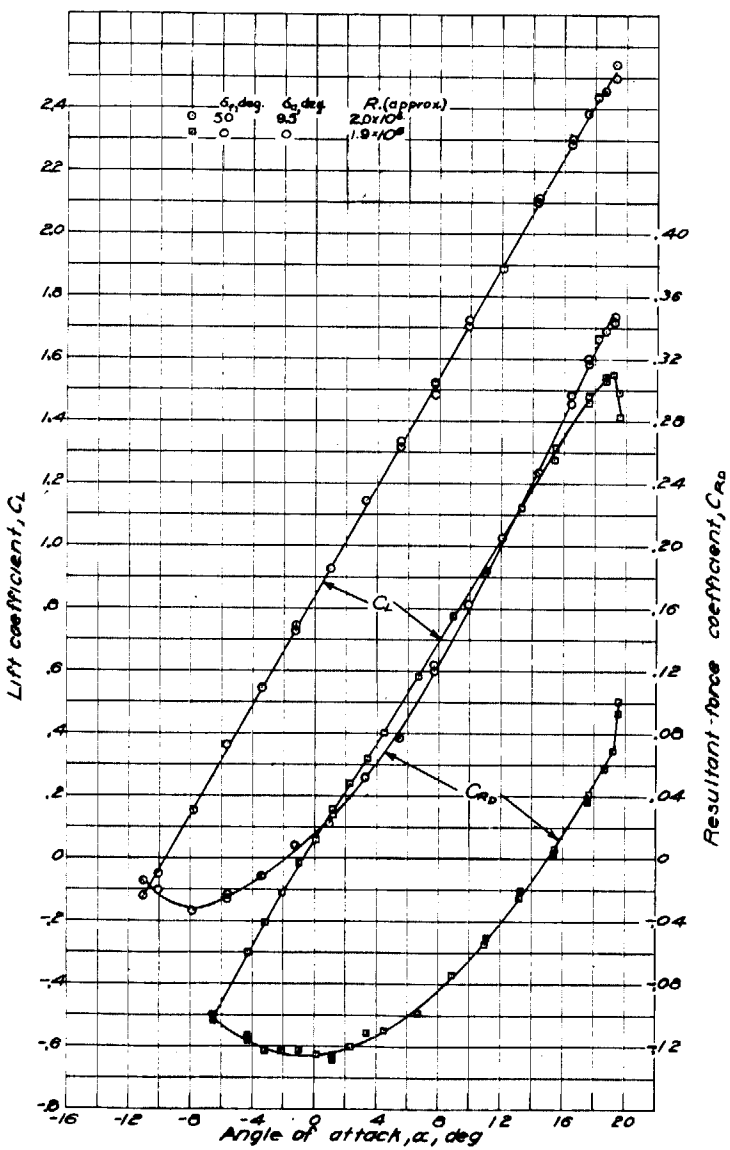

Figure 14 .-Variation of lift and resultant-force coefficients with angle of attack; power on; i_t = 1.6°; q≈13 lb/sq ft.

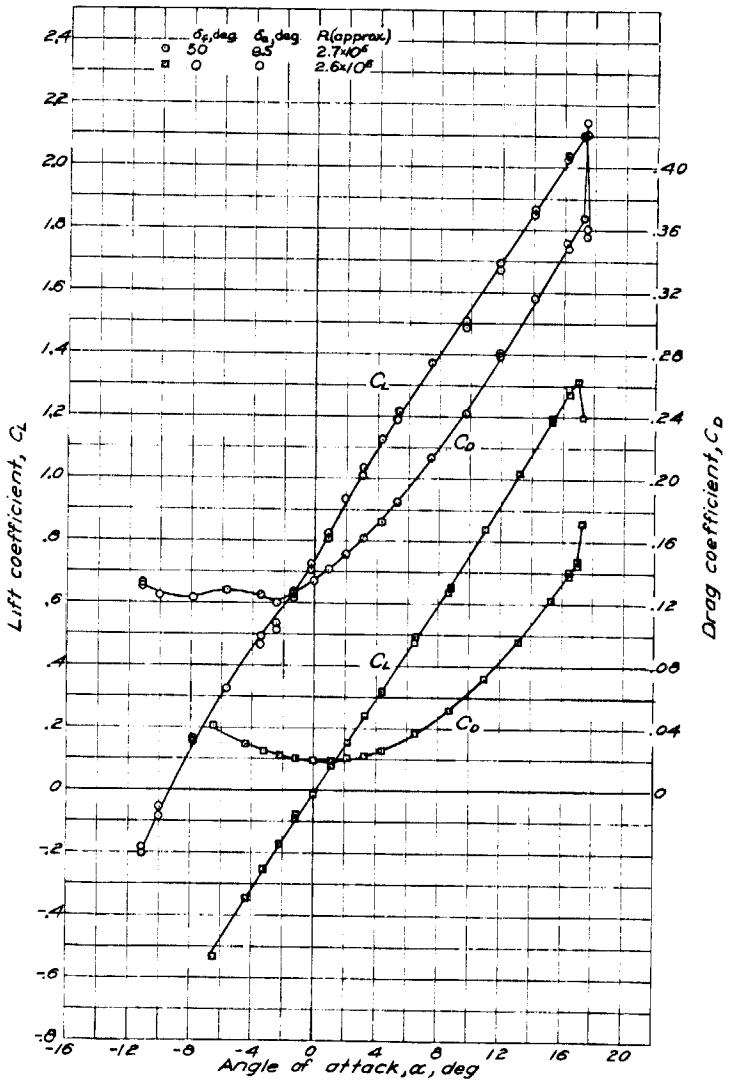

Figure 15 .-Variation of lift and drag coefficients with angle of attack; power off; i_t=-2.3°; q≈2.5 lb/sq ft.

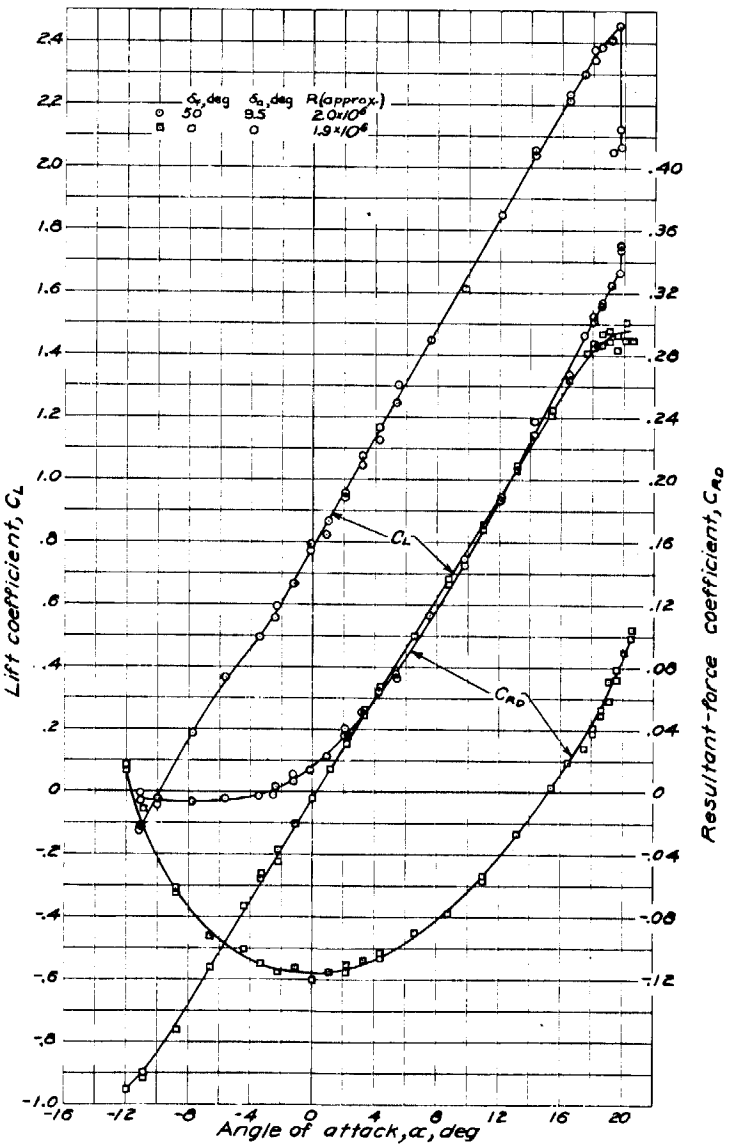

Figure 16.- Variation of lift and resultant-force coefficients with angle of attack; power on; i_t=-2.3°; q≈13 lb/sq ft

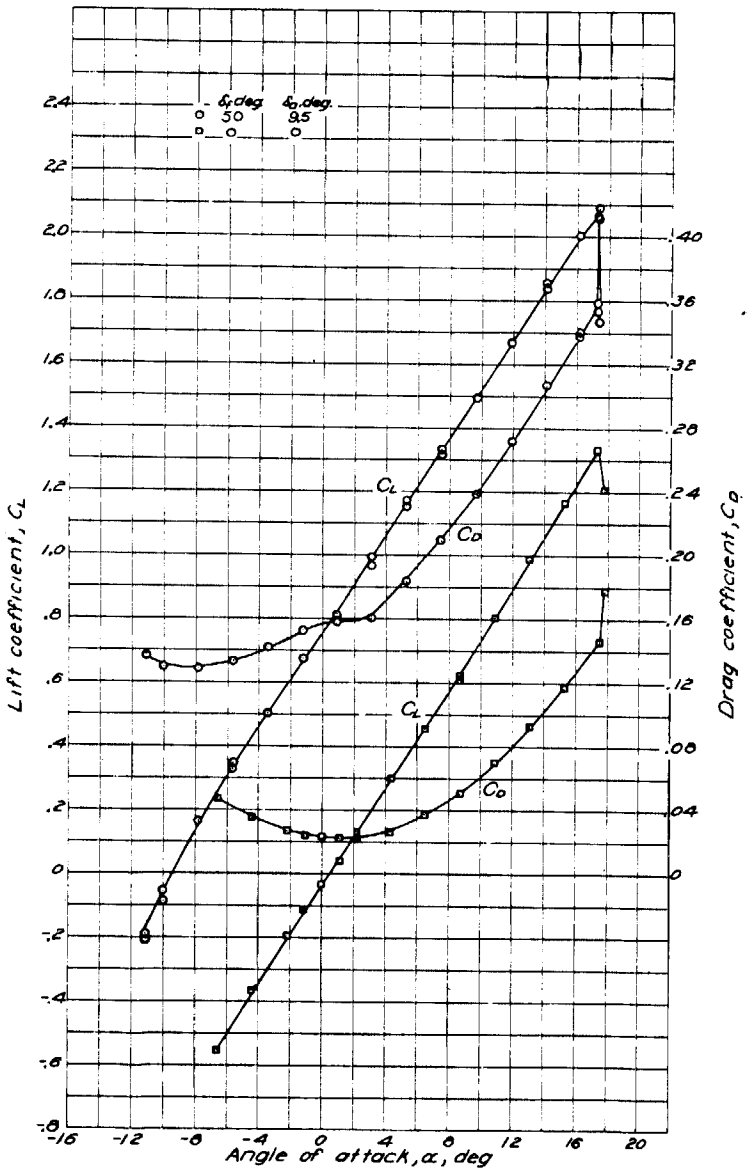

Figure 17 .-Variation of lift and drag coefficients with angle of attack; power off; $i_t = -5.0°$; $q = 25$ lb/sq ft; $R \approx 2.6 \times 10^6$

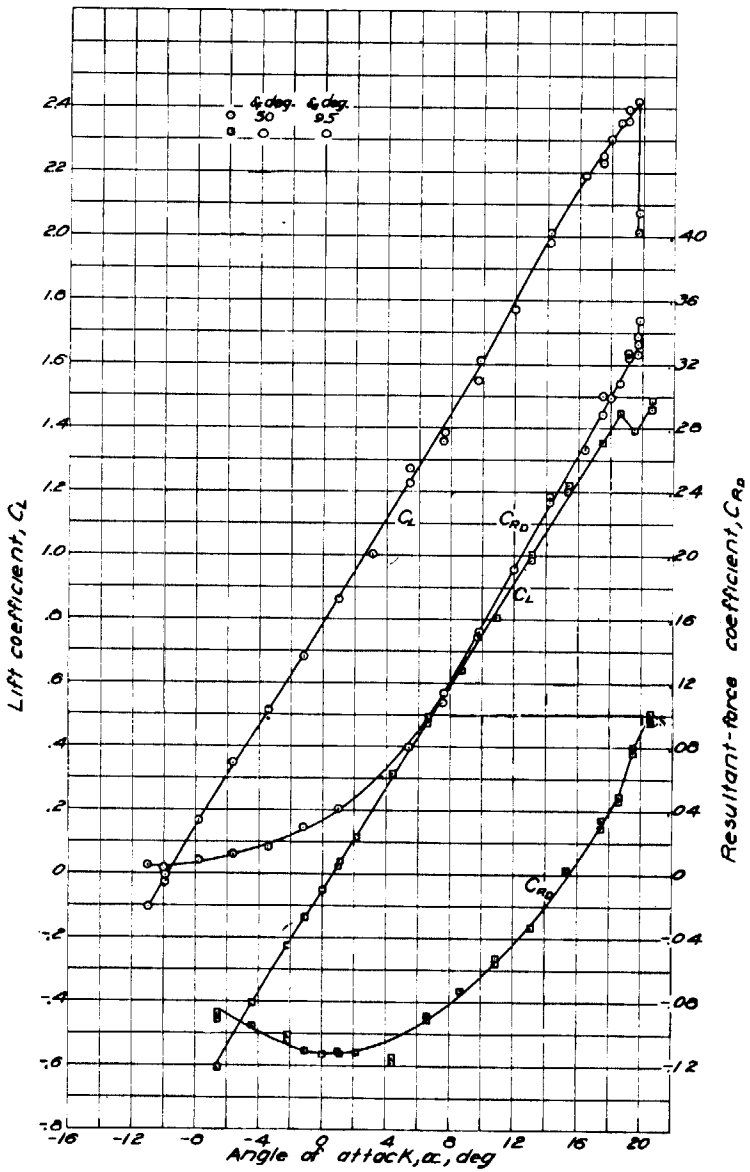

Figure 18 .-Variation of lift and resultant-force coefficients with angle of attack; power on; $i_t = -5.0°$; $q = 13$ lb/sq ft; $R \approx 1.9 \times 10^6$

NACA

Figs. 17, 18

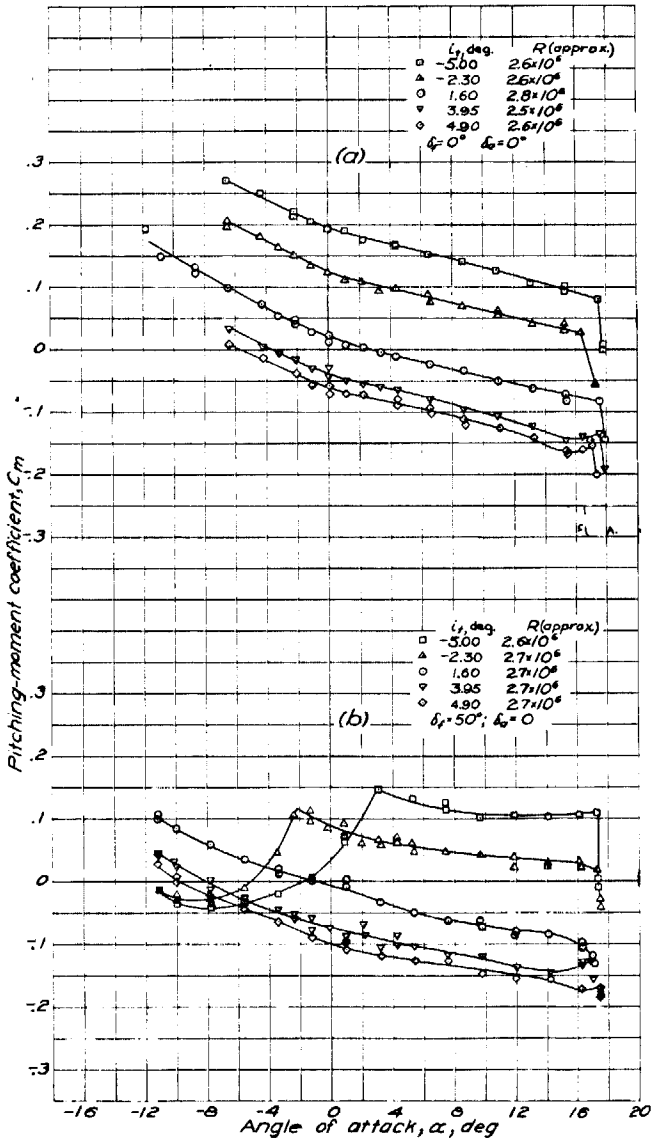

Figure 19 .-Variation of pitching-moment coefficient with angle of attack for several stabilizer angles; power off; q=25 lb/sq ft.

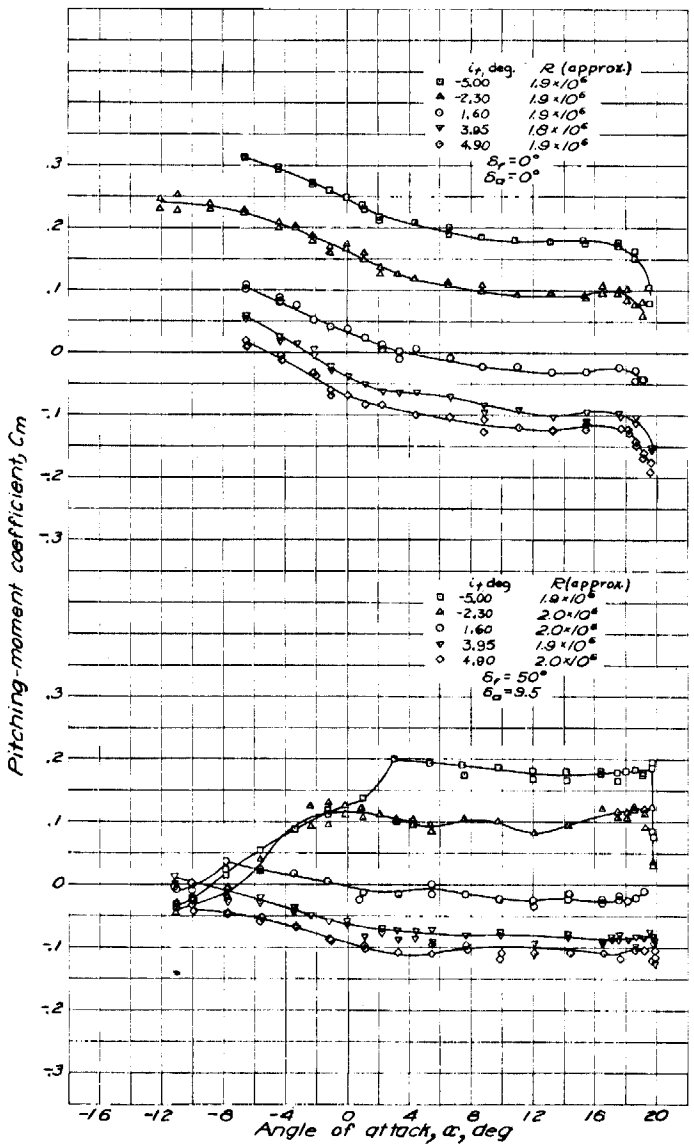

Figure 20 .-Variation of pitching-moment coefficient with angle of attack for several stabilizer angles; power on; q=13 lb/sq ft.

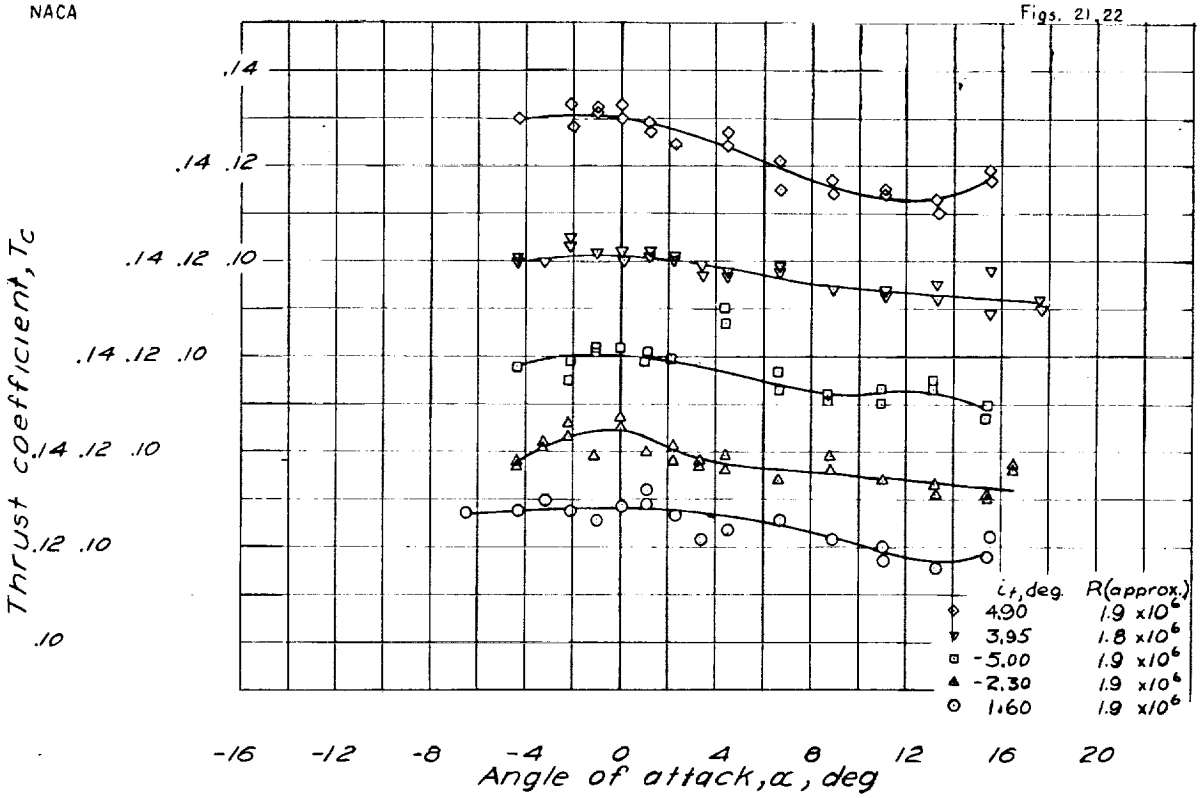

Figure 21.— Variation of thrust coefficient with angle of attack. Power on; $\delta_f = 0°$; $\delta_a = 0°$; $q \approx 13$ lb/sq ft.

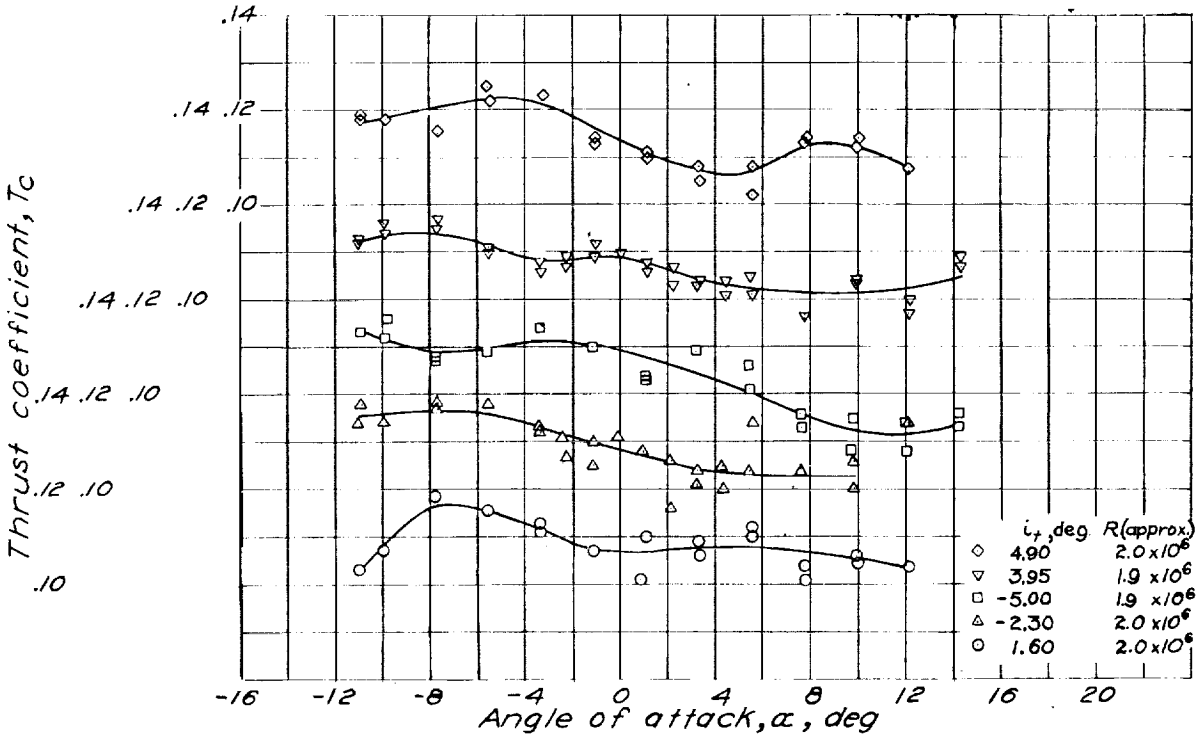

Figure 22 .-Variation of thrust coefficient with angle of attack. Power on; $\delta_f = 50°$; $\delta_a = 9.5°$; $q \approx 13$ lb/sq ft.

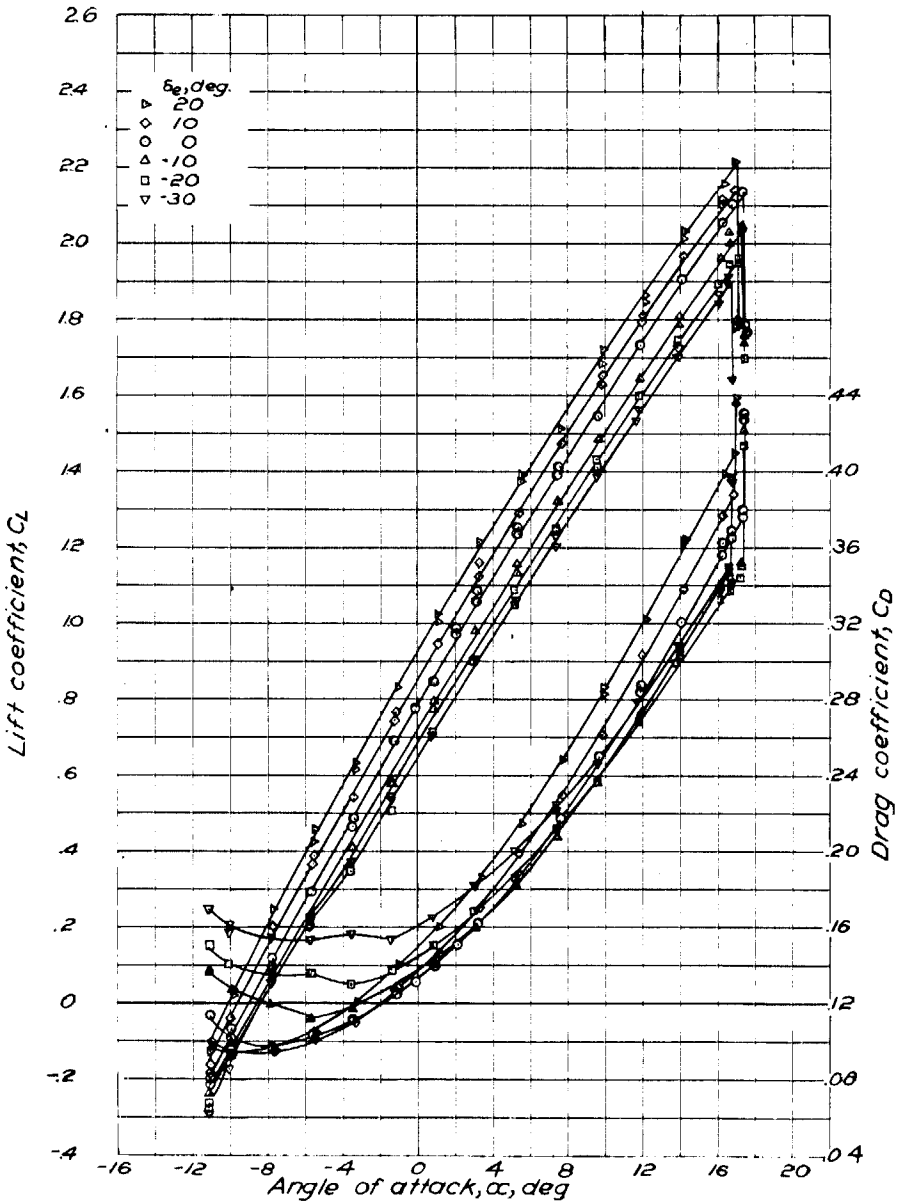

Figure 23.- Variation of lift and drag coefficients with angle of attack for elevator nose 5; power off; i_t=1.5°; δ_f=50°; δ_a=9.5°; $q \approx 25$ lb/sq ft; $R \approx 26 \times 10^6$

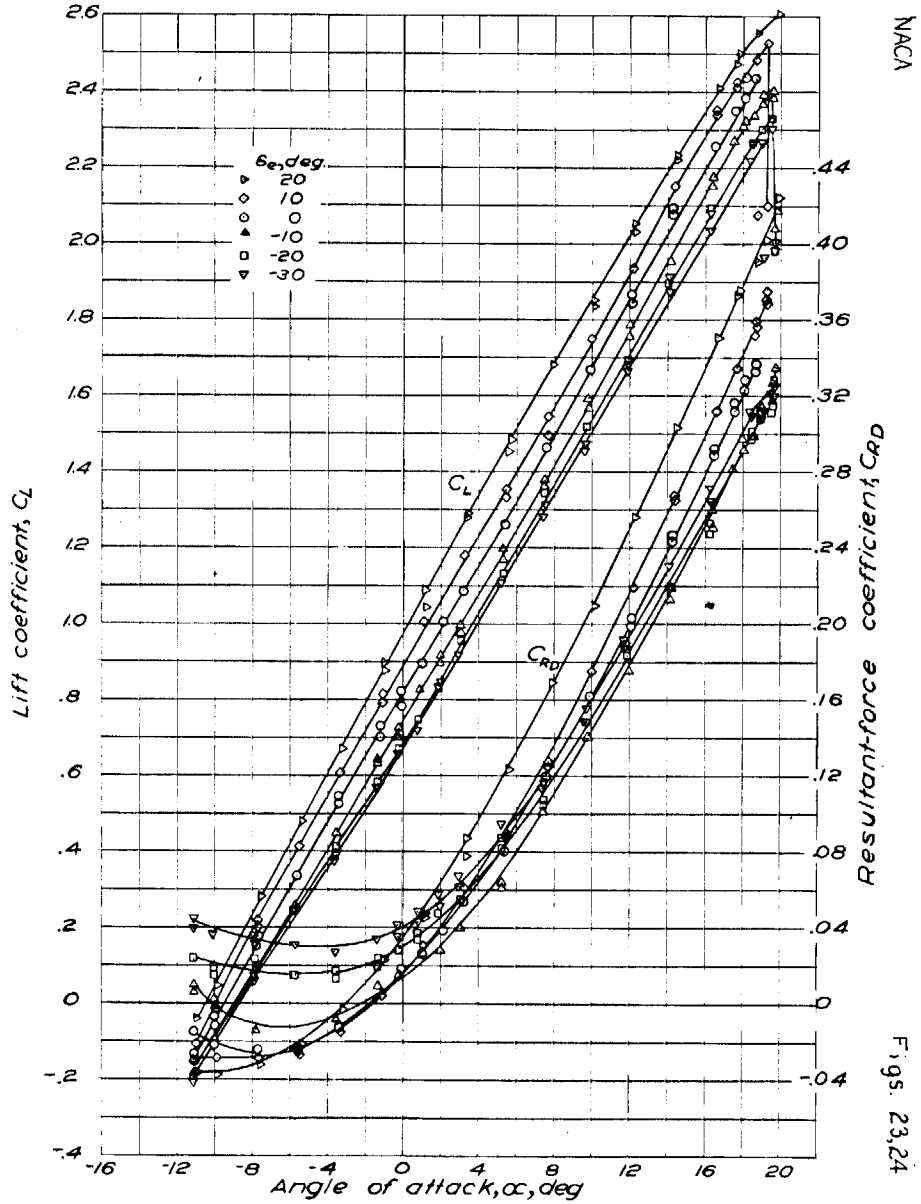

Figure 24.- Variation of lift and resultant-force coefficients with angle of attack for elevator nose 5; power on; i_t=1.5°; δ_f=50°; δ_a=9.5°; $q \approx 13$ lb/sq ft; $R \approx 1.9 \times 10^6$

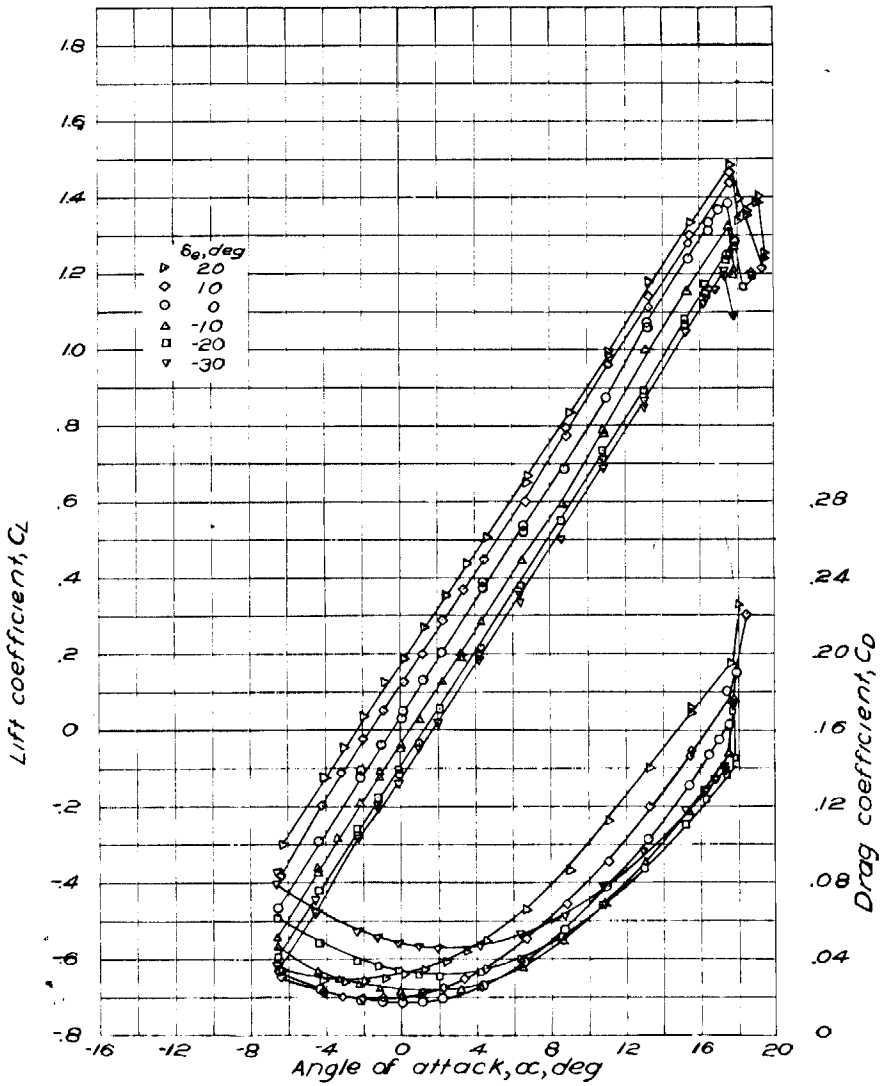

Figure 25.-Variation of lift and drag coefficients with angle of attack for elevator nose 5; power off; i_t=1.5°; δ_f=0°; δ_a=0°; q≈25 lb/sq ft; R≈2.7×10⁶

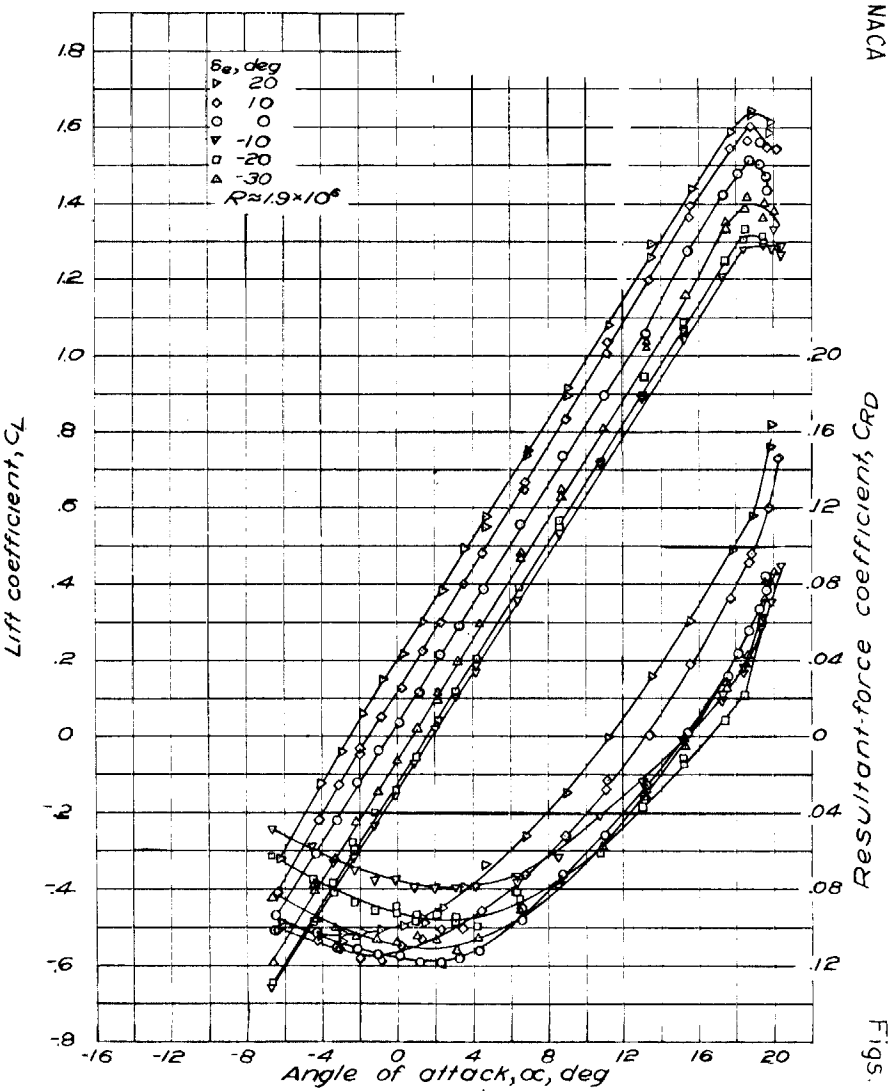

Figure 26.-Variation of lift and resultant-force coefficients with angle of attack for elevator nose 5; power on; i_t=1.5°; δ_f=0°; δ_a=0°; q≈13 lb/sq ft.

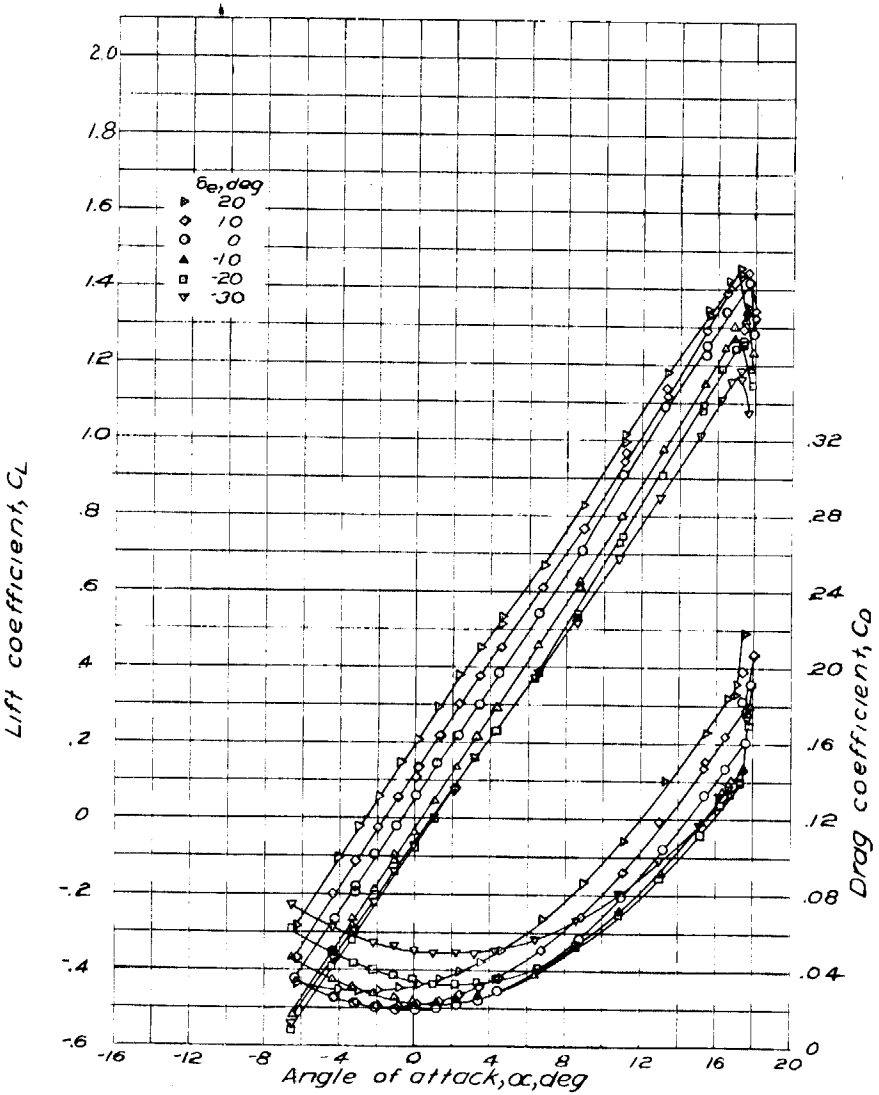

Figure 27.–Variation of lift and drag coefficient with angle of attack for elevator nose 1; power off; i_t 1.5°; δ_f=0°; δ_a=0°; q≈25 lb/sq ft; R≈2.7×10⁶.

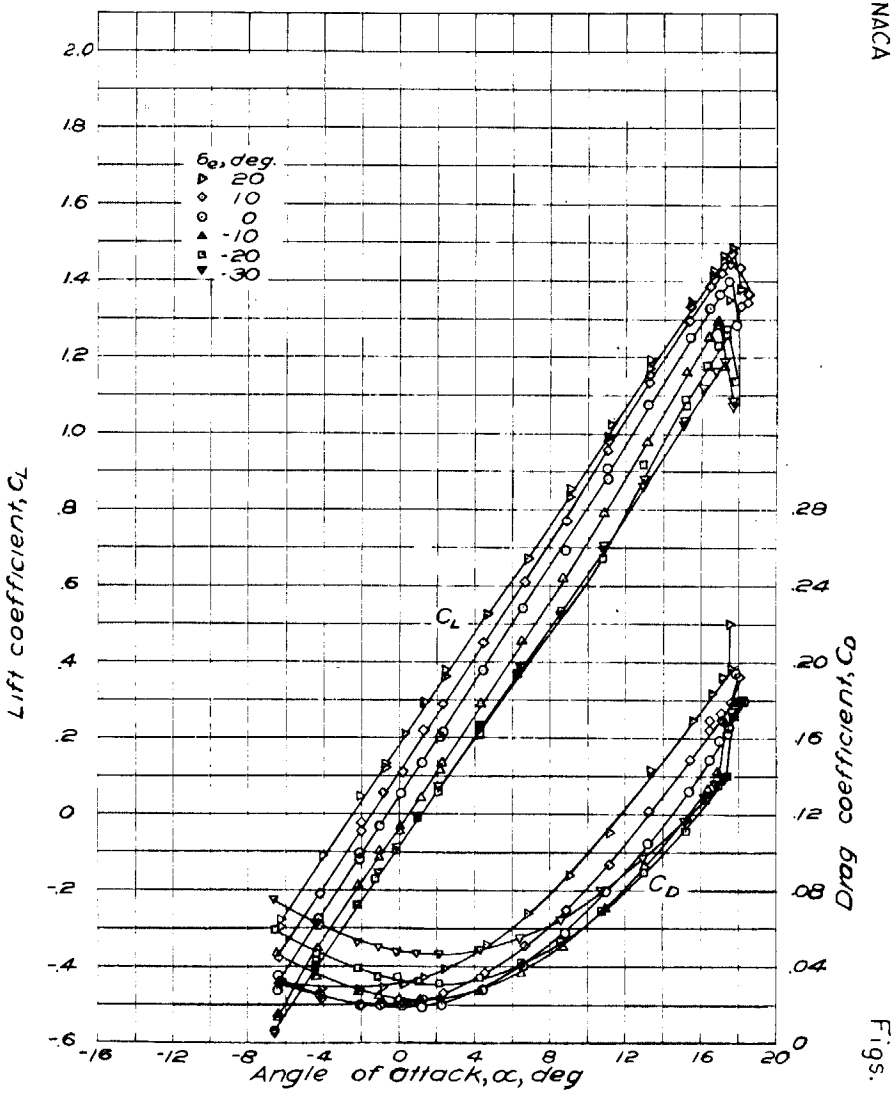

Figure 28.–Variation of lift and drag coefficients with angle of attack for elevator nose 2; power off; i_t=1.5°; δ_f=0°; δ_a=0°; q=25 lb/sq ft; R≈2.6×10⁶.

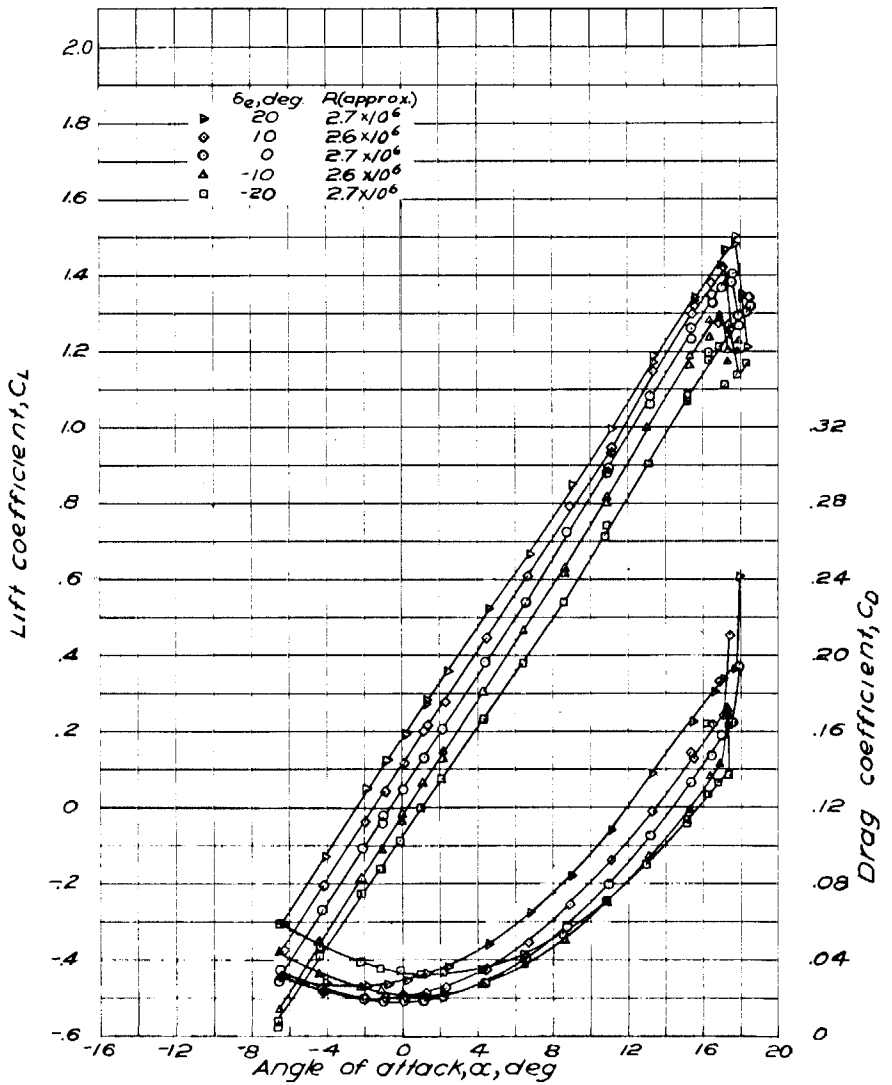

Figure 29.- Variation of lift and drag coefficients with angle of attack for elevator nose 3; power off; i_t=1.5°; δ_f=0°; δ_a=0°; q≈25 lb/sq ft.

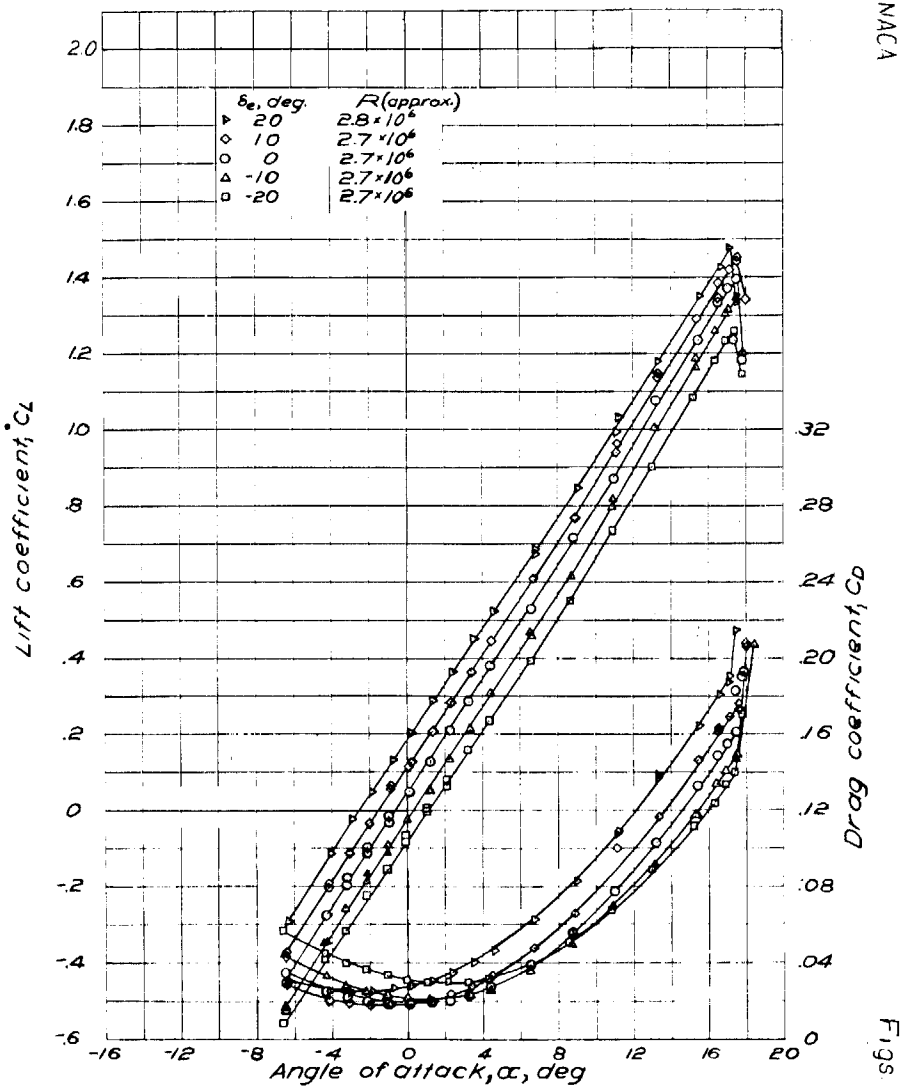

Figure 30.- Variation of lift and drag coefficients with angle of attack for elevator nose 4; power off; i_t=1.5°; δ_f=0°; δ_a=0°; q≈25 lb/sq ft.

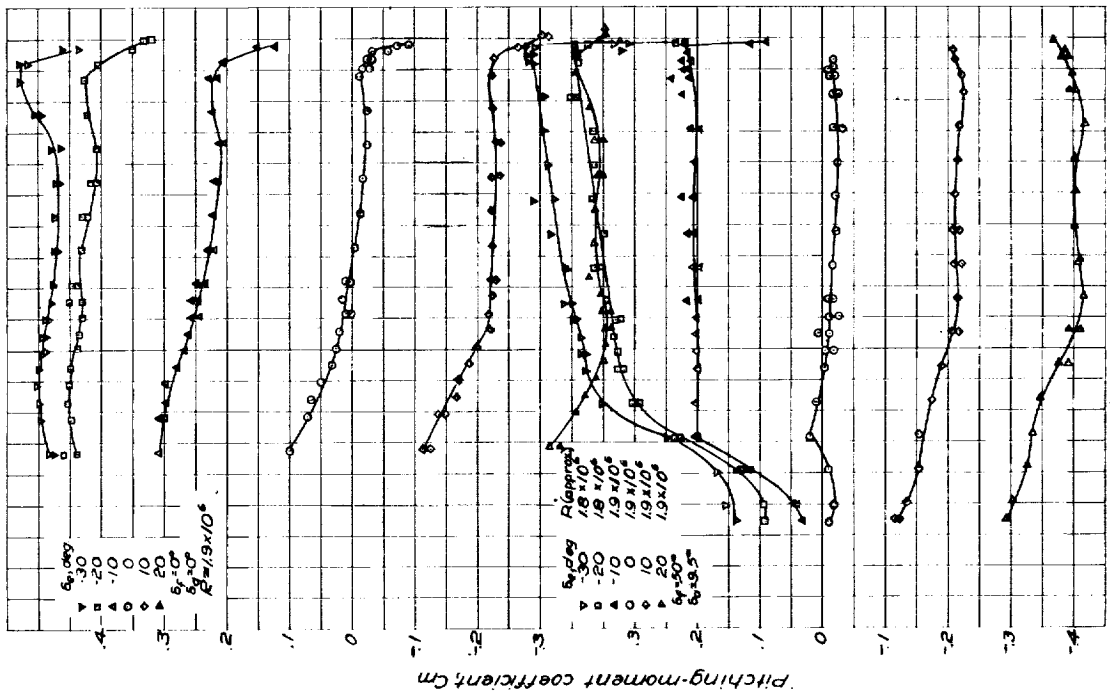

Figure 32.-Variation of pitching-moment coefficient with angle of attack for elevator nose 5; power off; i_t=1.5°; δ_f=0°, 50°; δ_s=0°, 9.5°; i_t=1.5°; q=13 lb/sq ft.

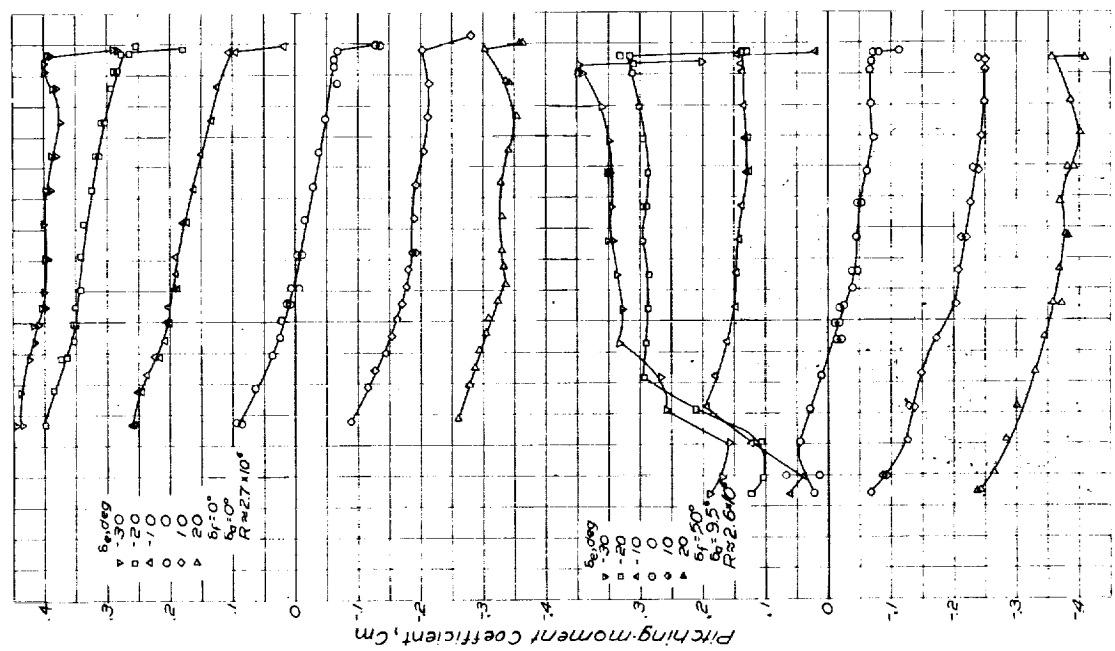

Figure 31.-Variation of pitching-moment coefficient with angle of attack for elevator nose 5; power off; i_t=1.5°; δ_f=0°, 50°; δ_s=0°, 9.5°; i_t=1.5°; q=25 lb/sq ft.

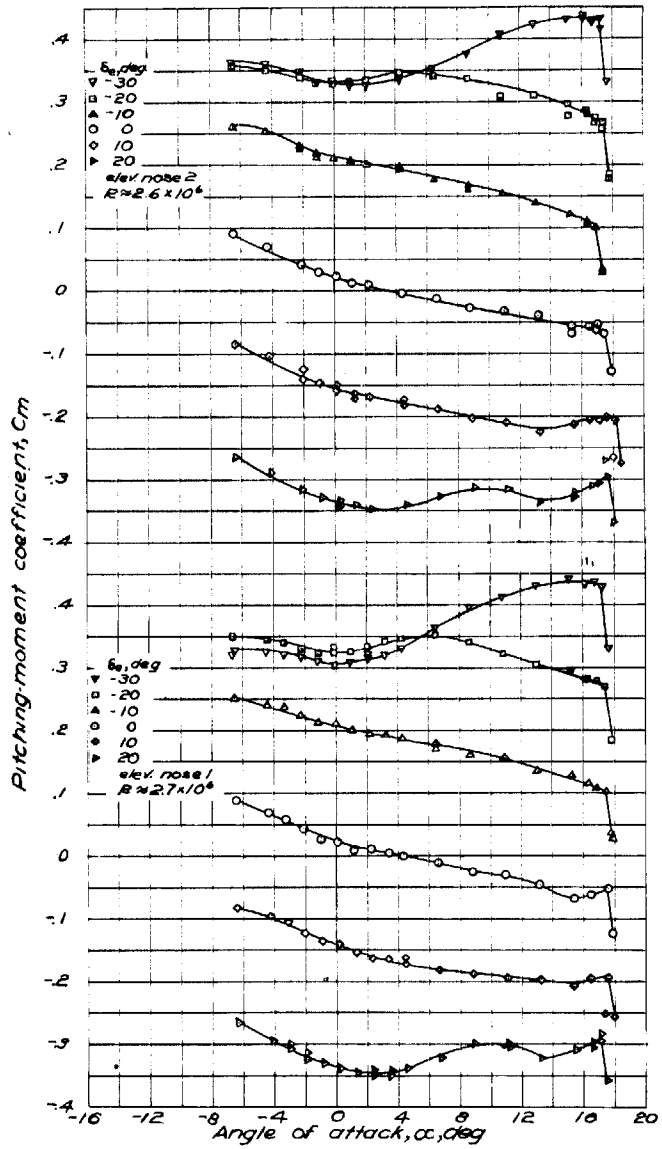

Figure 33.-Variation of pitching-moment coefficient with angle of attack for elevator nose 1 and 2; power off; i_t=1.5°; δ_f=0°; δ_a=0°; q≈25 lb/sq ft.

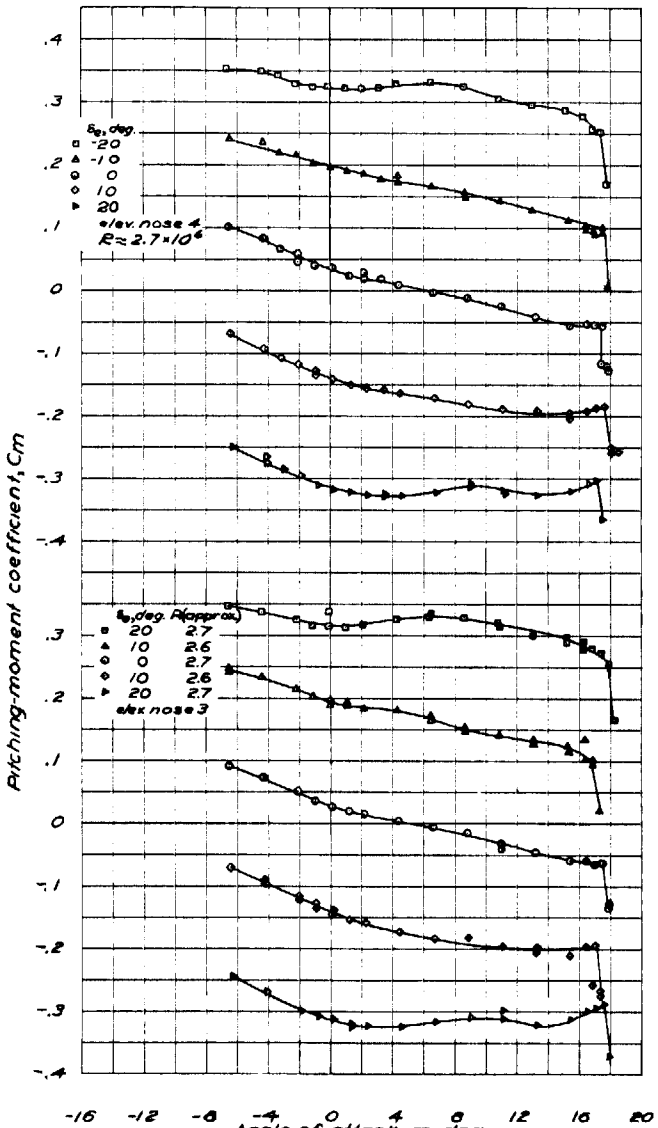

Figure 34.-Variation of pitching-moment coefficient with angle of attack for elevator nose 3 and 4; power off; i_t=1.5°; δ_f=0°; δ_a=0°; q≈25 lb/sq ft.

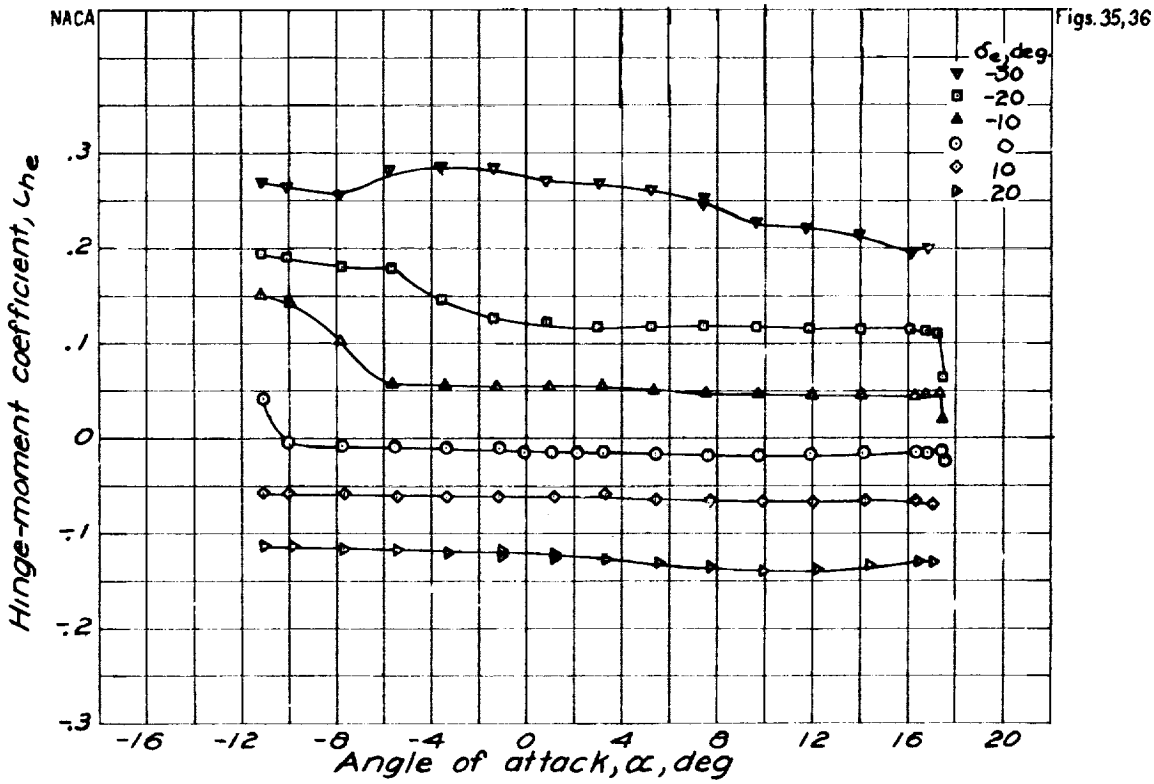

Figure 35 .-Variation of elevator hinge-moment coefficient with angle of attack for elevator nose 5; power off; $i_t = 1.5°$; $\delta_f = 50°$; $\delta_a = 9.5°$; $q \approx 25$ lb/sq ft.; $R \approx 2.6 \times 10^6$

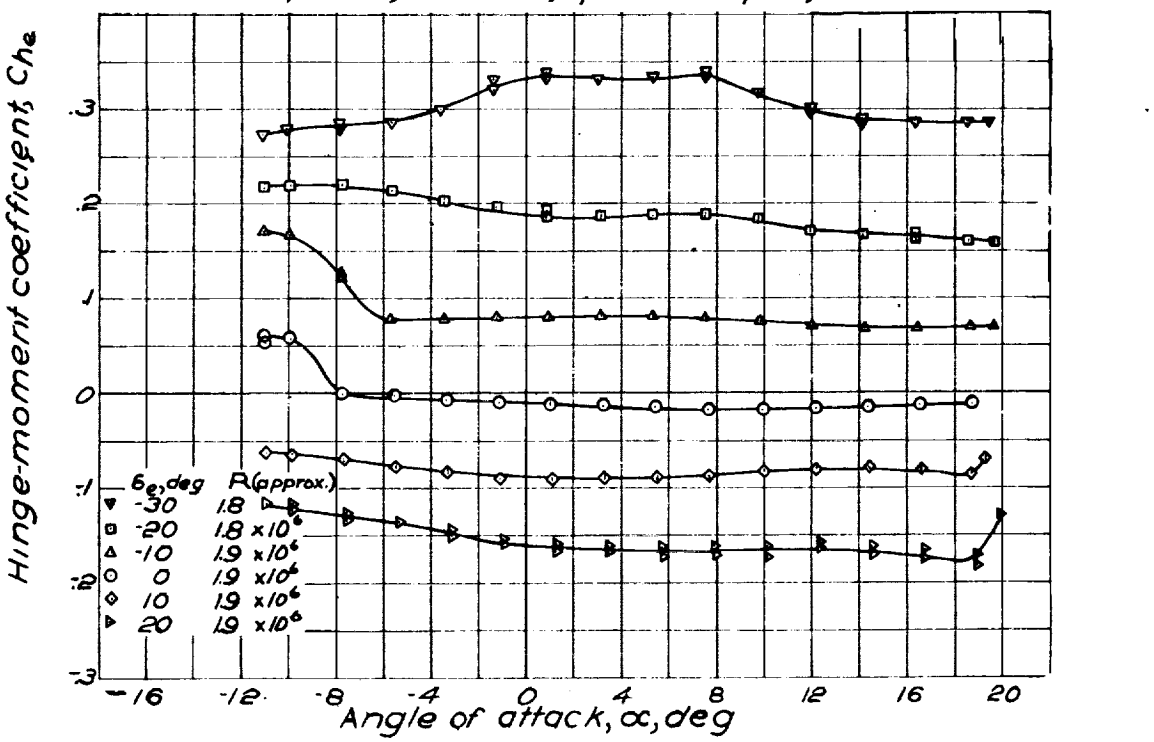

Figure 36.-Variation of elevator hinge-moment coefficient with angle of attack for elevator nose 5; power on $i_t = 1.5°$; $\delta_f = 50°$; $\delta_a = 9.5°$; $q \approx 13$ lb/sq ft.

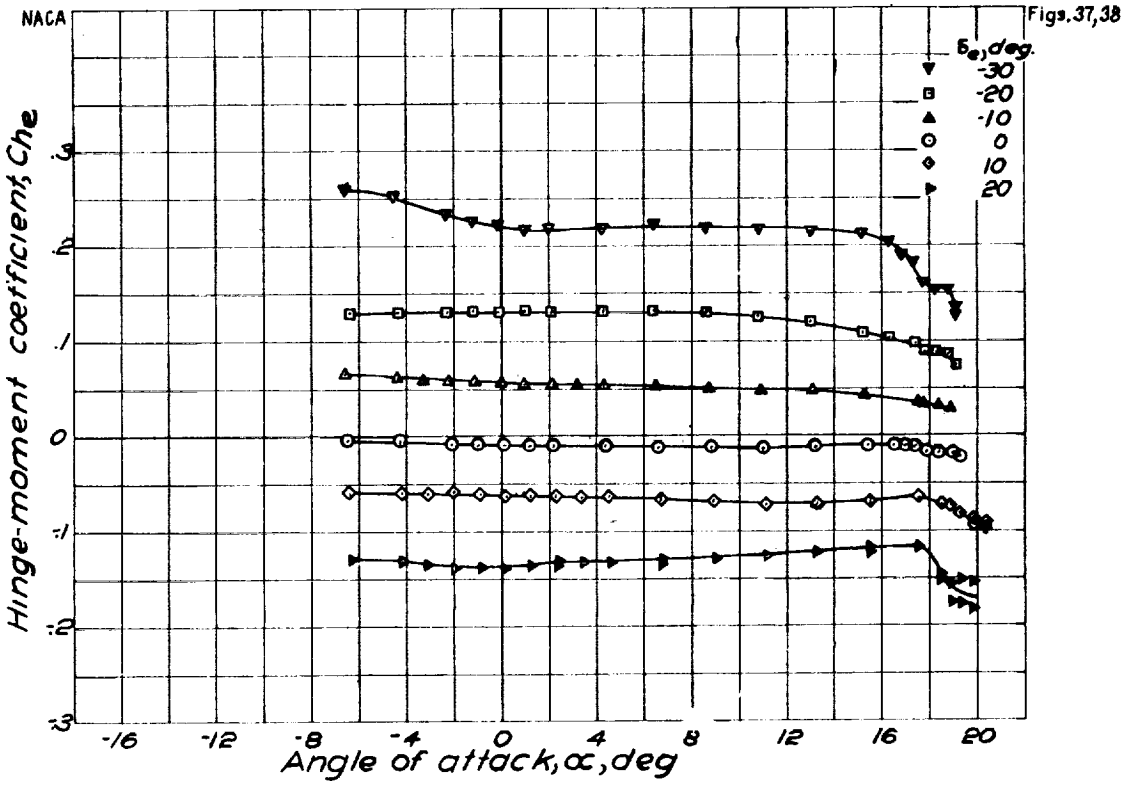

Figure 37.- Variation of elevator hinge-moment coefficient with angle of attack for elevator nose 5; power off; $i_t = 1.5°$; $\delta_f = 0°$; $\delta_a = 0°$; $q \approx 25$ lb/sq ft; $R \approx 2.7 \times 10^6$

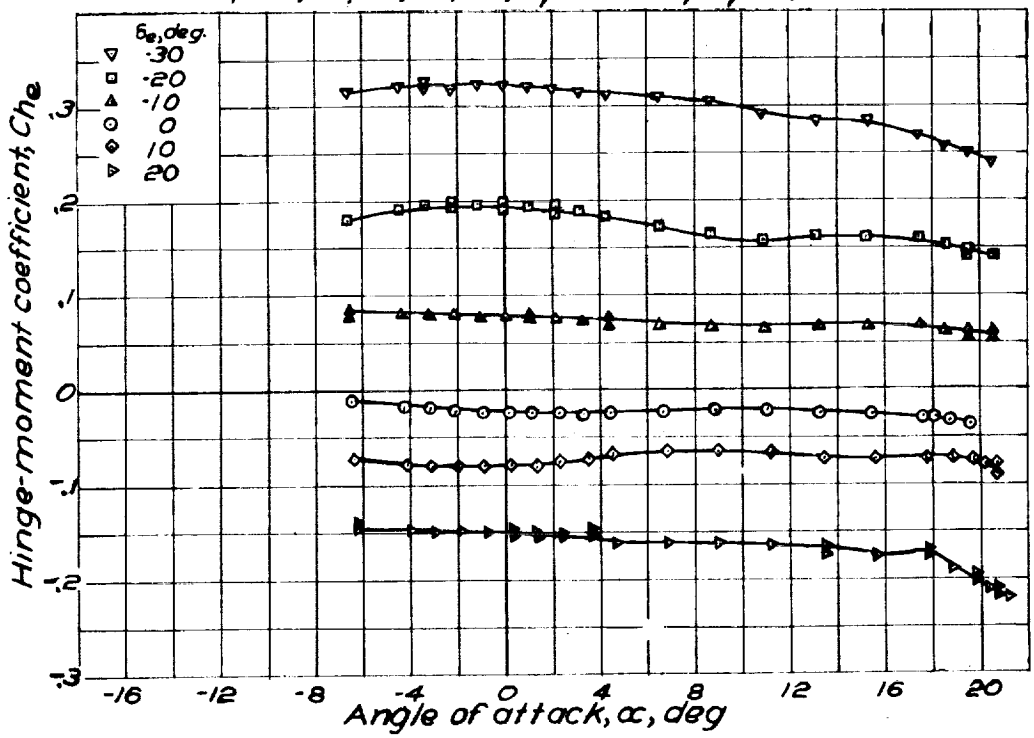

Figure 38.- Variation of elevator hinge-moment coefficient with angle of attack for elevator nose 2; power on; $i_t = 1.5°$; $\delta_f = 0°$; $\delta_a = 0°$; $q \approx 13$ lb/sq ft; $R \approx 1.9 \times 10^6$

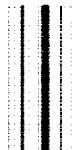

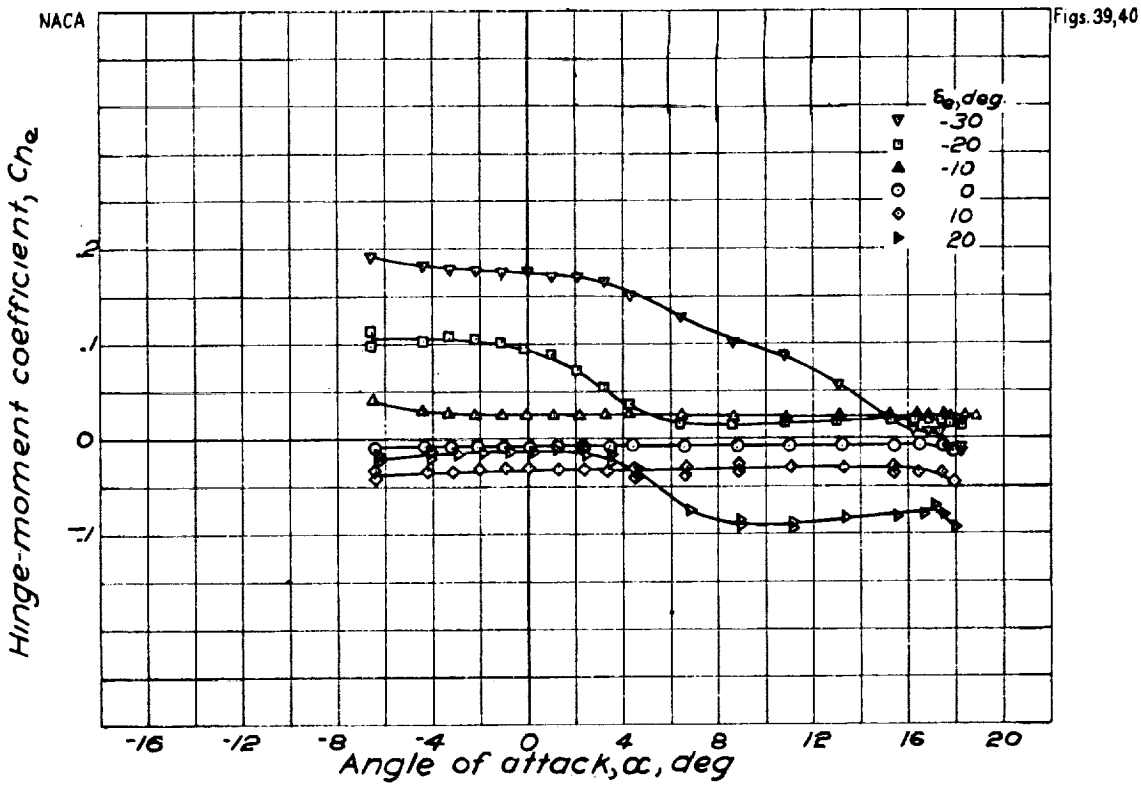

Figure 39.-Variation of elevator hinge-moment coefficient with angle of attack for elevator nose 1; power off; $i_t = 1.5°$; $\delta_f = 0°$; $\delta_a = 0°$; $q \approx 25$ lb/sq ft; $R \approx 2.7 \times 10^6$

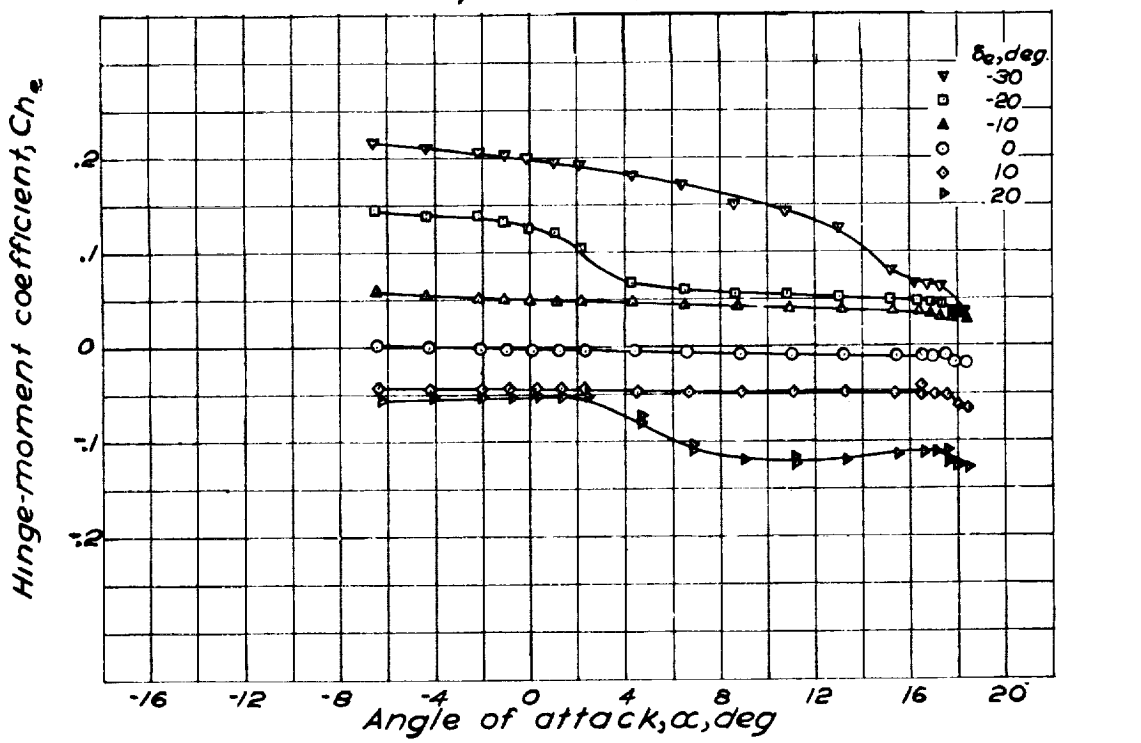

Figure 40.-Variation of elevator hinge-moment coefficient with angle of attack for elevator nose 2; power off; $i_t = 1.5°$; $\delta_f = 0°$; $\delta_a = 0°$; $q \approx 25$ lb/sq ft.; $R \approx 2.6 \times 10^6$

L-440

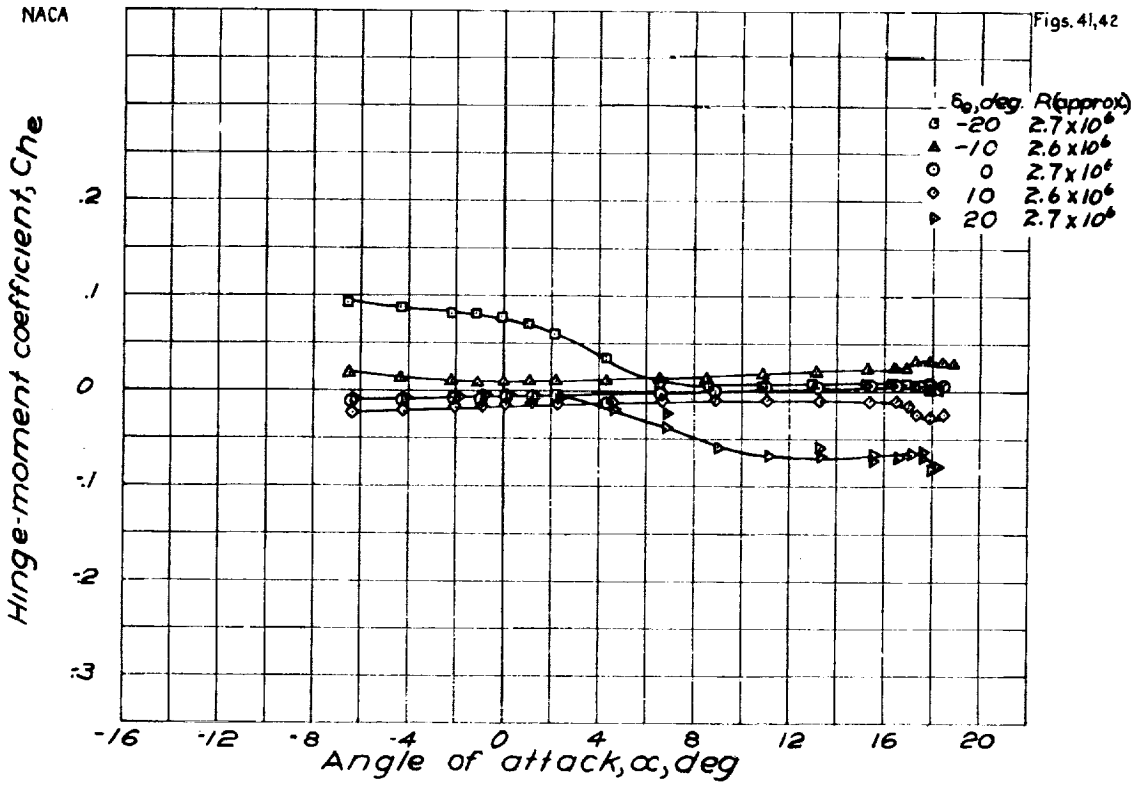

Figure 41.-Variation of elevator hinge-moment coefficient with angle of attack for elevator nose 3; power off; $i_t = 1.5°$; $\delta_f = 0°$; $\delta_a = 0°$; $q \approx 25$ lb/sq ft.

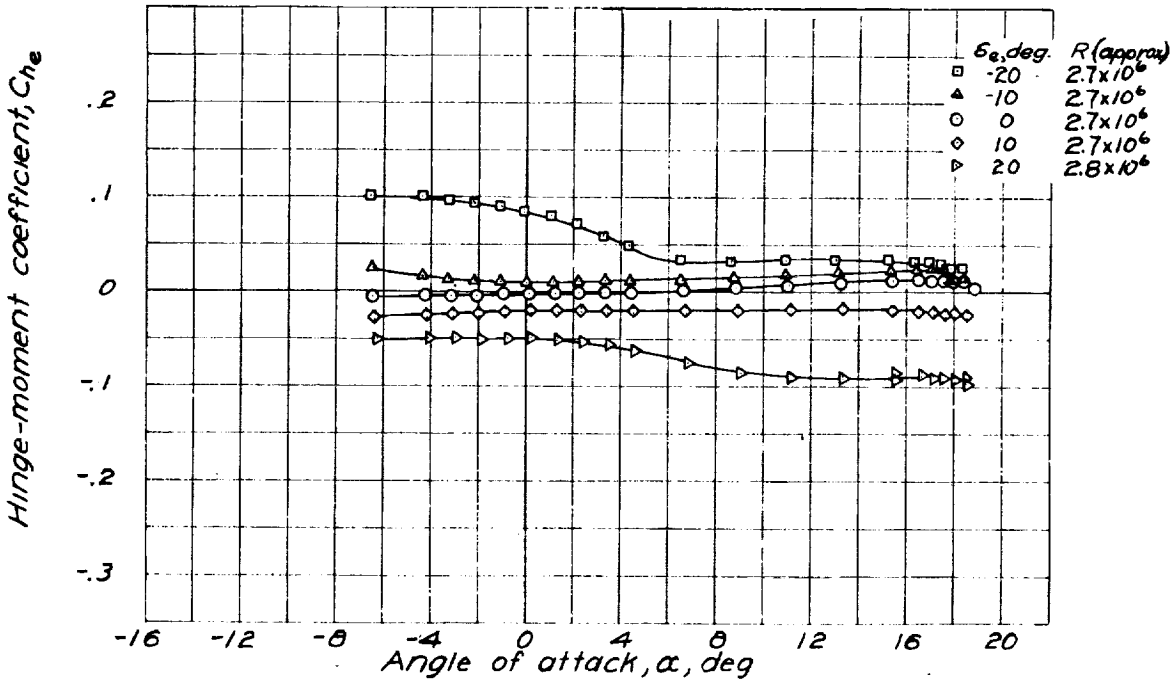

Figure 42.-Variation of elevator hinge-moment coefficient with angle of attack for elevator nose 4; power off; $i_t = 1.5°$; $\delta_f = 0°$; $\delta_a = 0°$; $q \approx 25$ lb/sq ft.

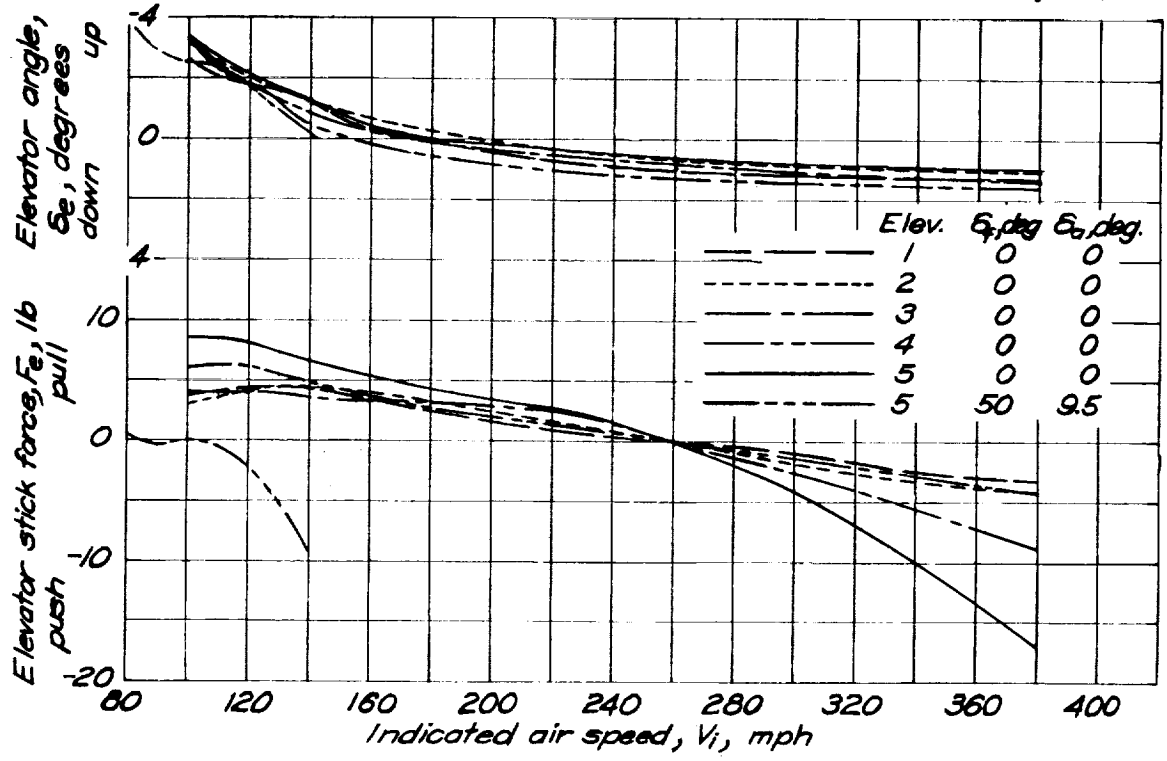

Figure 43.– Variaton of elevator stick force with indicated air speed for several elevator noses; power off; $i_t = 1.5°$.

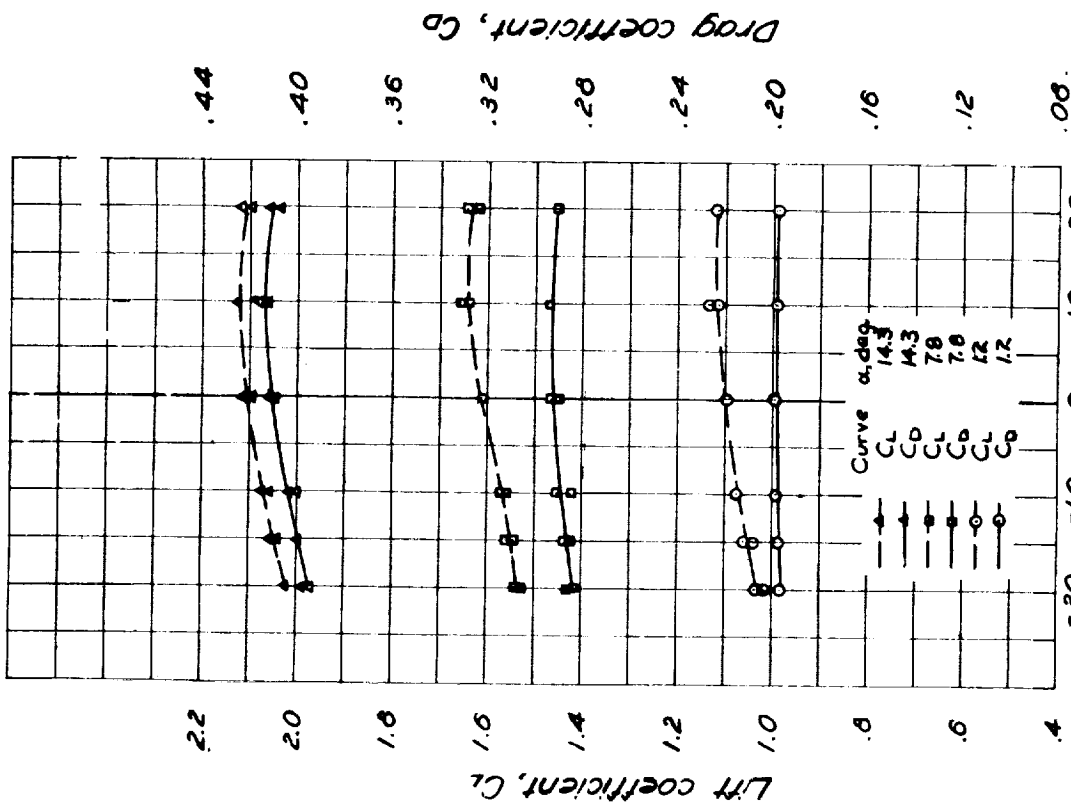

Figure 50.–Variation of lift and drag coefficients with right aileron deflection; power off; $i_t = 1.5°$; $\delta_f = 20°$; $\delta_{fsp} = 48°$; $\delta_{a_l} = 0°$; $q = 25$ lb/sq.ft.; $R = 2.5 \times 10^6$.

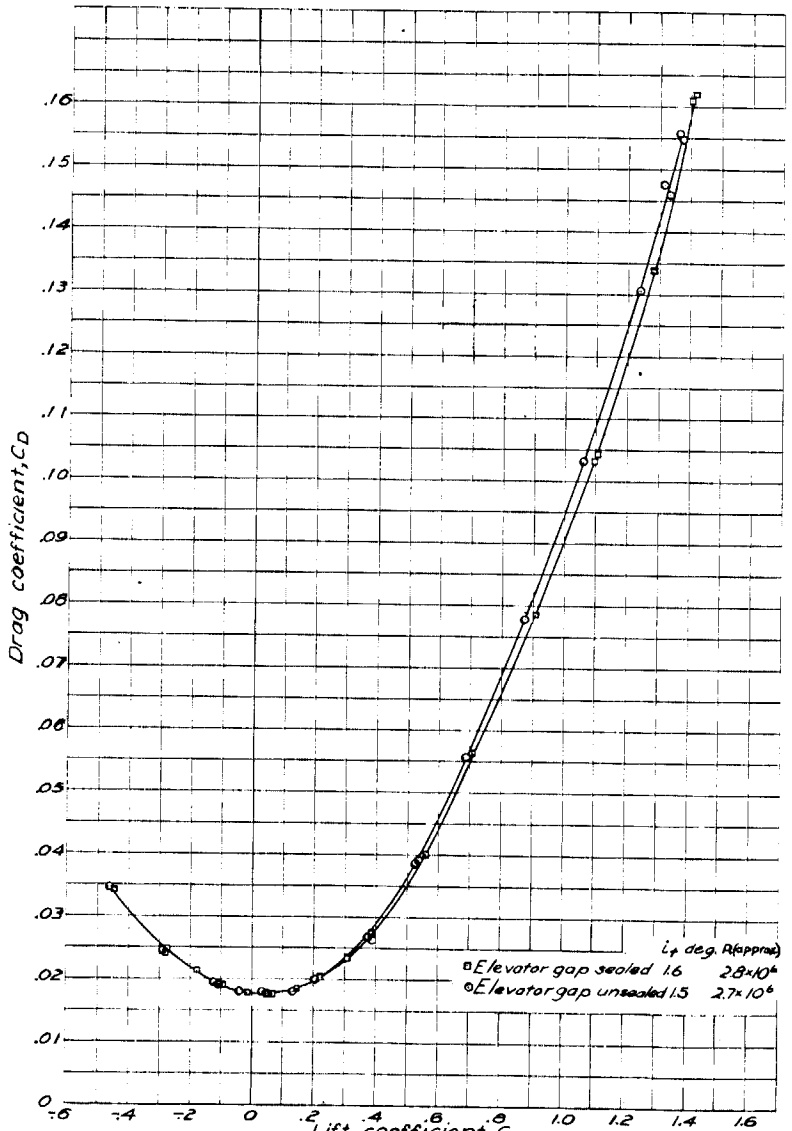

Figure 44.--Effect of sealing the gap between the stabilizer and elevator on lift and drag coefficients; power off; δ_f=0°; δ_a=0°; q=25 lb/sq ft.

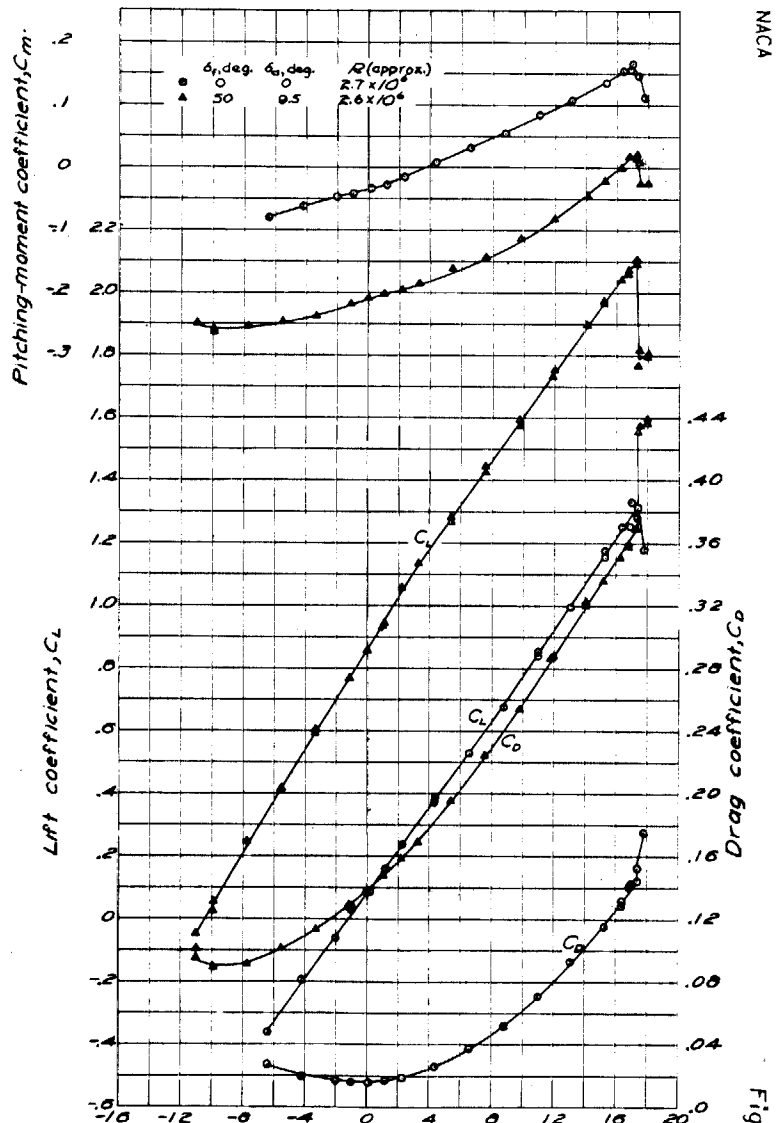

Figure 45.--Variation of lift, drag, and pitching-moment coefficients with angle of attack; horizontal tail off; power off; q=23 lb/sq ft.

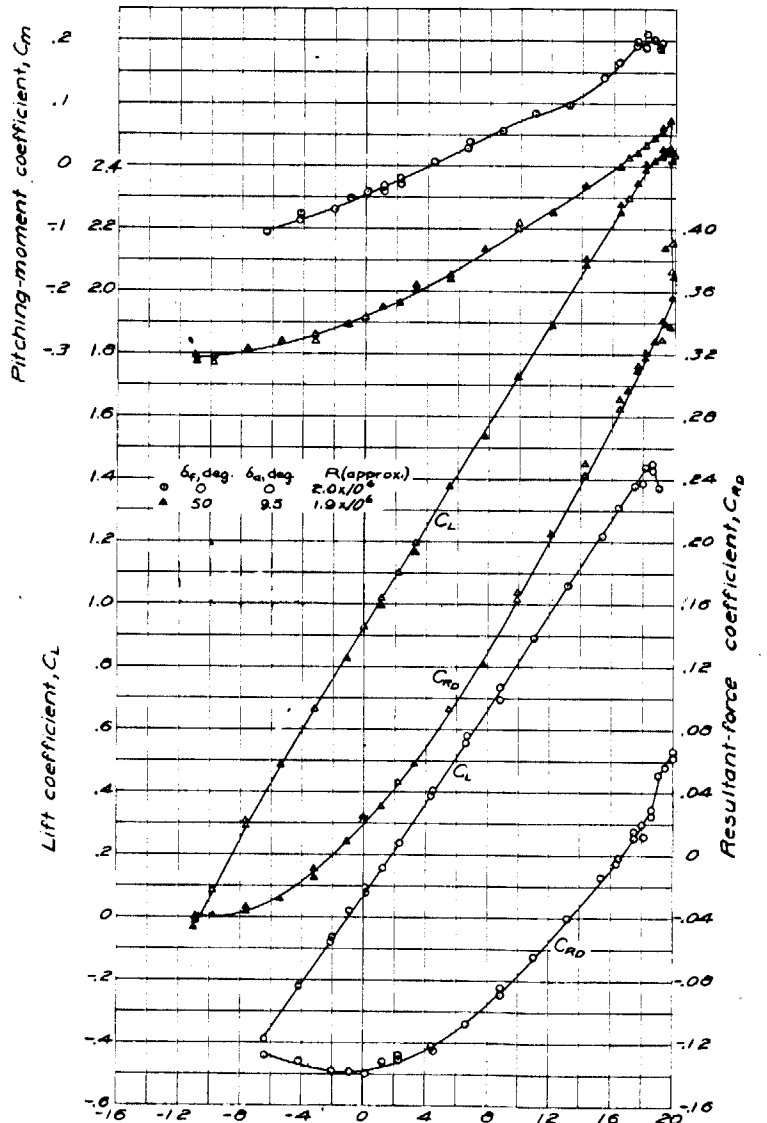

Figure 46.- Variation of lift, resultant-force, and pitching-moment coefficients with angle of attack; horizontal tail off; power on; $\beta = 15°$; $q \approx 13$ lb/sq ft.

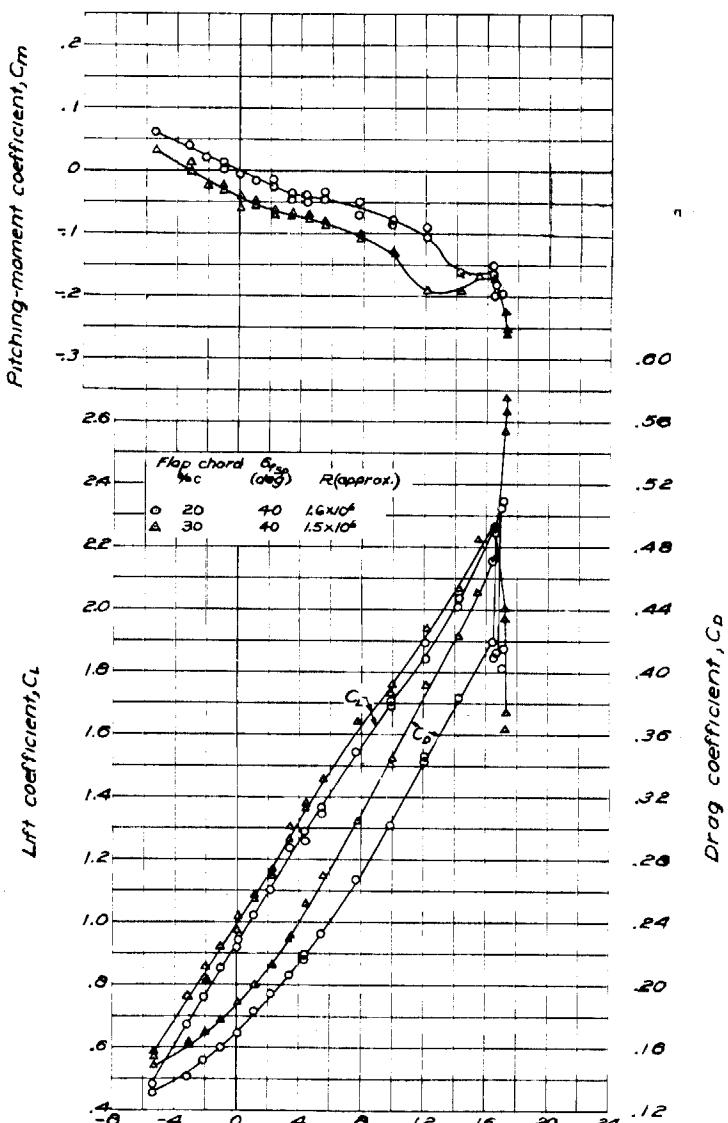

Figure 47.- Variation of lift, drag, and pitching-moment coefficient with angle of attack; power off; $i_t = 1.6°$; $\delta_f = 50°$; $\delta_a = 0°$; $q \approx 8.4$ lb/sq ft.

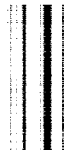

L-440

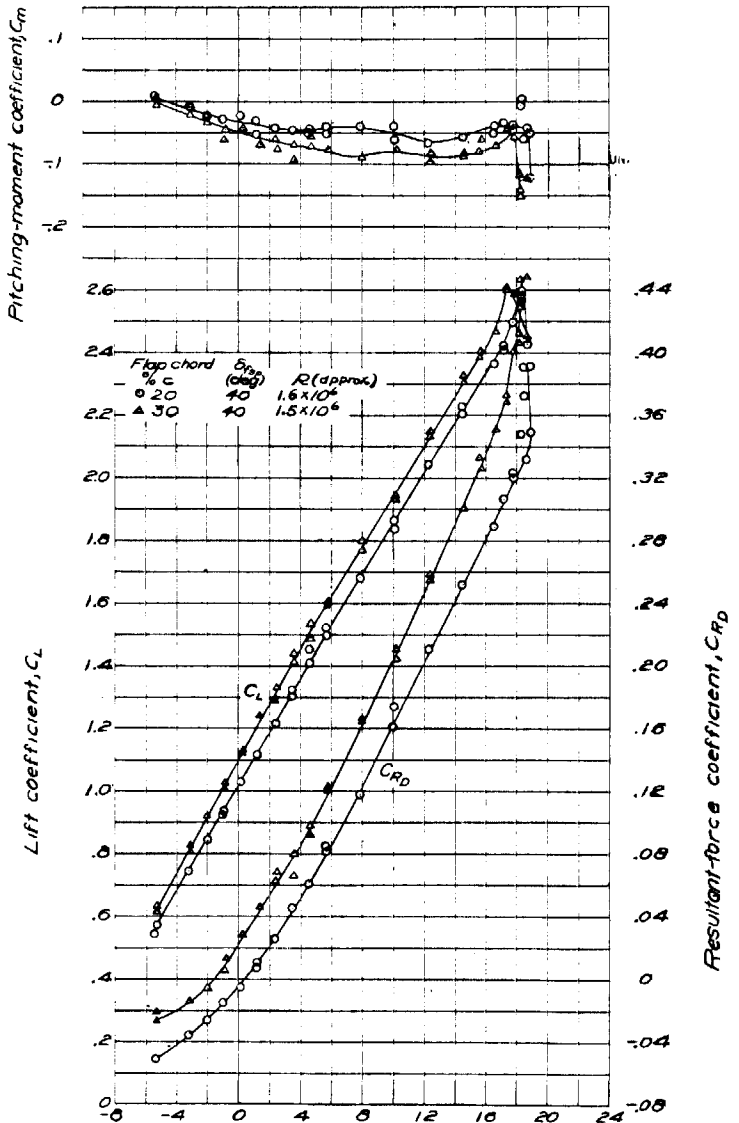

Figure 48 :-Variation of lift, resultant force and pitching-moment coefficients with angle of attack; power on; β=20°; i_t=1.6°; δ_f=50°; δ_a=0°; q=8.4 lb/sq ft.

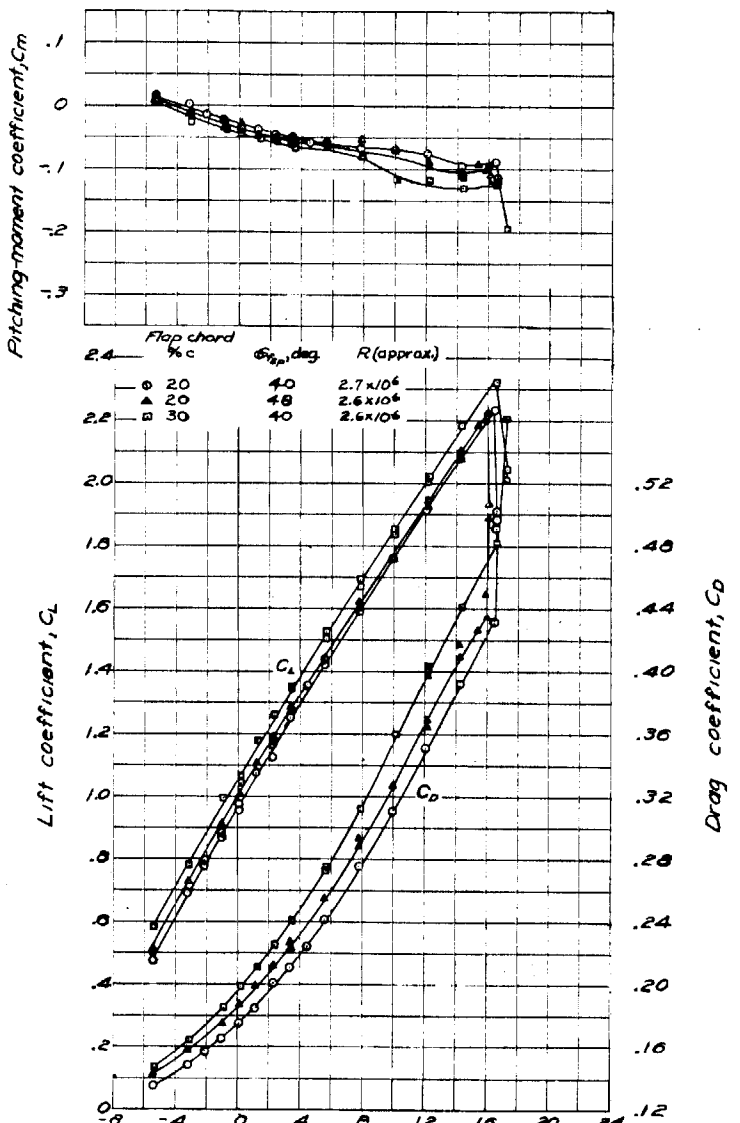

Figure 49 :-Variation of lift, drag, and pitching-moment coefficients with angle of attack; power off; i_t=1.6°; δ_f=50°; δ_a=0°; q=25 lb/sq ft.

NACA

Figs. 48,49

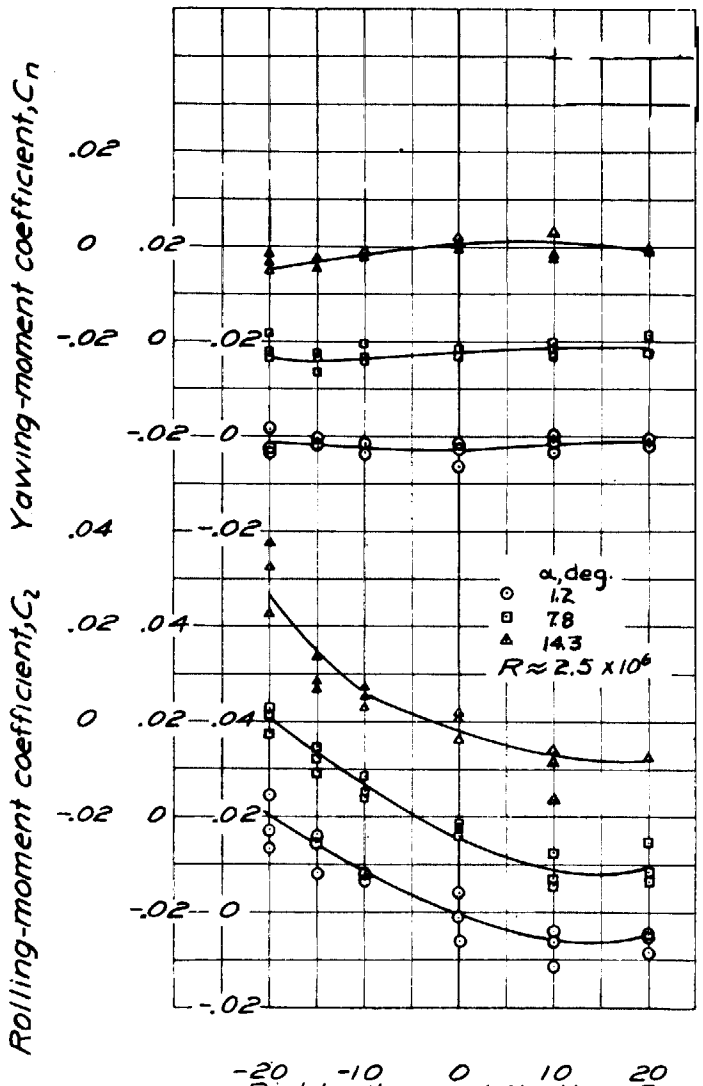

Figure 51.-Variation of rolling-moment and yawing-moment coefficients with right aileron deflection; power off; $i_t = 1.6°$; $\delta_f = 50°$; .20c; $\delta_{f\,SP} = 48°$; $\delta_{a_l} = 0°$; $q \approx 25$ lb/sq ft.

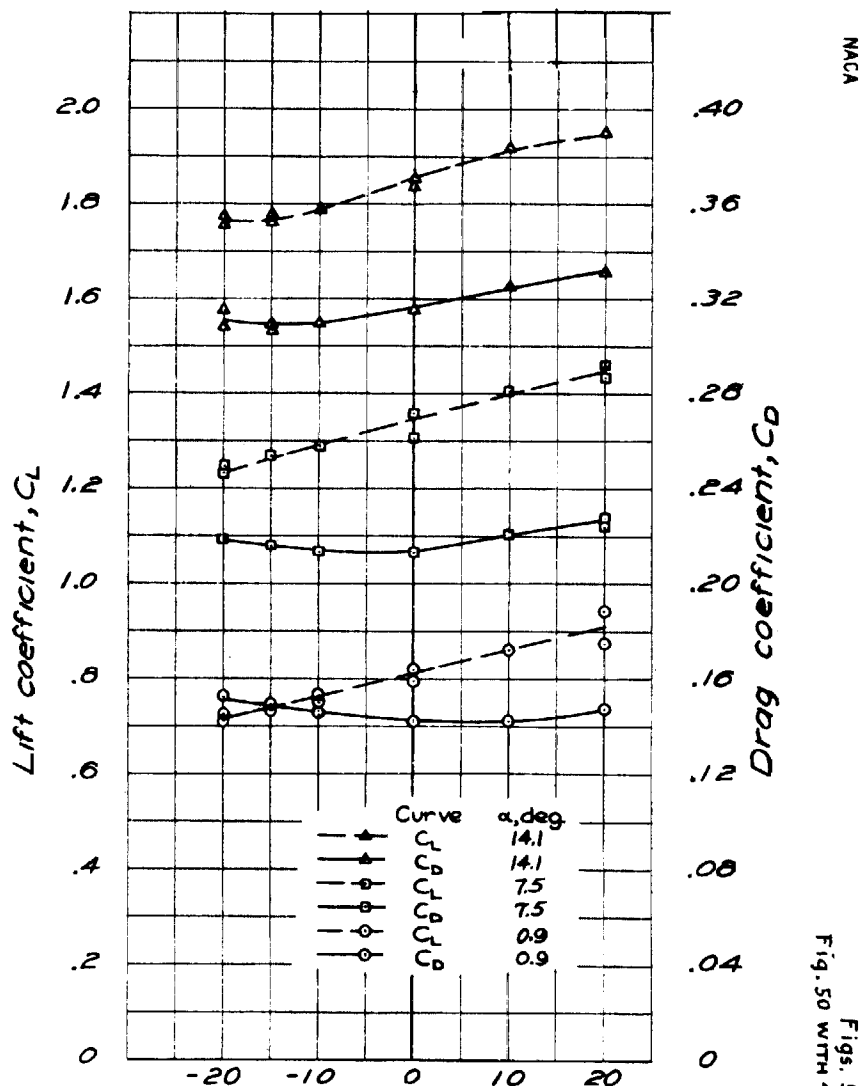

Figure 52.-Variation of lift and drag coefficients with right aileron deflection; power off; $i_t = 1.6°$; $\delta_f = 50°$; $\delta_{a_l} = 9.5°$; $q \approx 25$ lb/sq ft; $R \approx 2.7 \times 10^6$.

NACA

Figs. 51, 52 with 43

Fig. 50

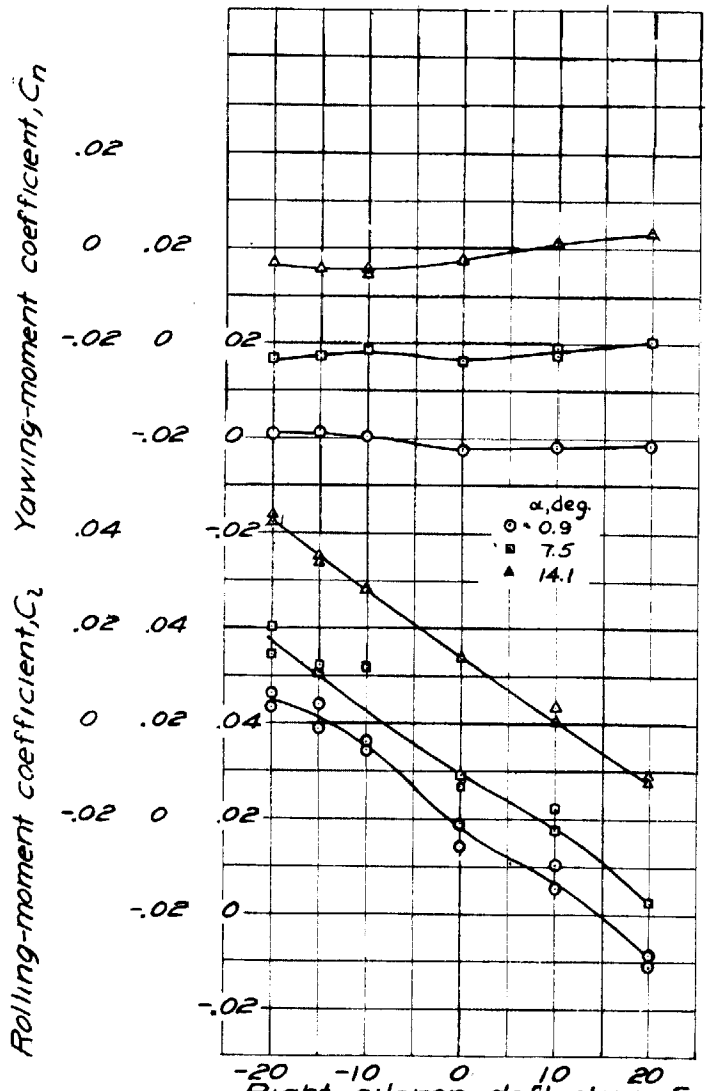

Figure 53.-Variation of rolling-moment and yawing-moment coefficients with right aileron deflection; power off; $i_t = 1.6°$; $\delta_f = 50°$; $\delta_{f_{SP}} = 0°$; $\delta_{a_l} = 9.5°$; $q \approx 25$ lb/sq ft.; $R \approx 2.7 \times 10^6$.

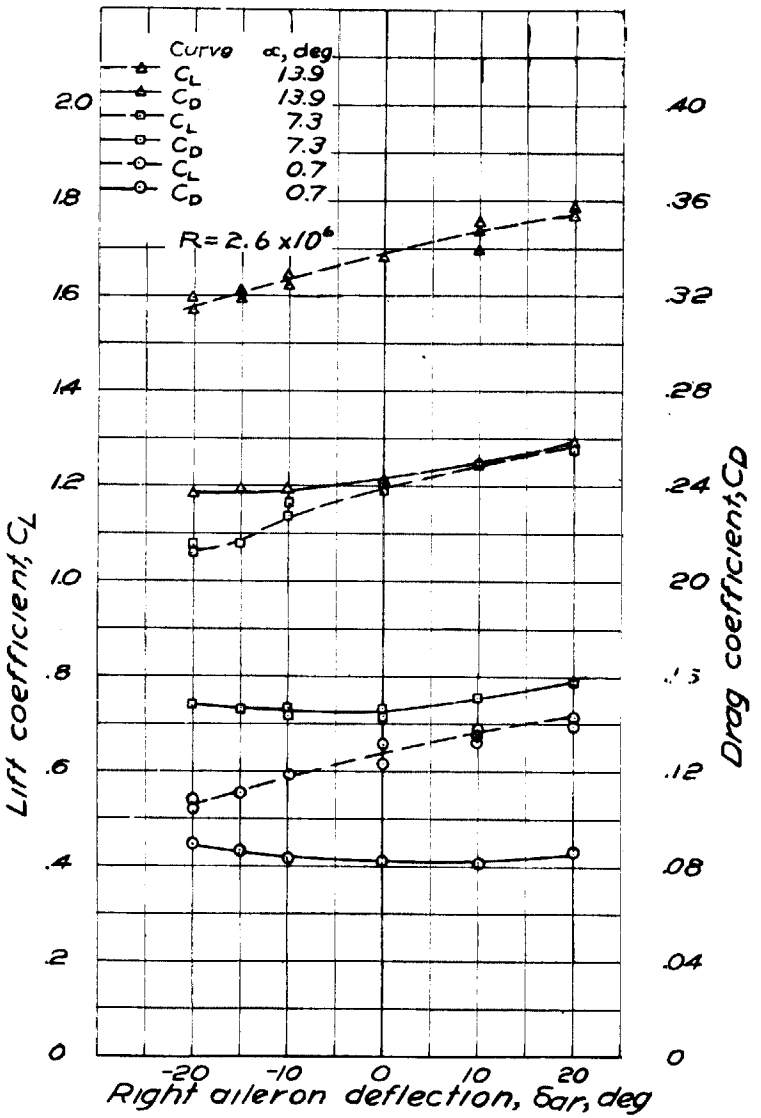

Figure 54.-Variation of lift and drag coefficients with right aileron deflection, power off; $i_t = 1.6°$; $\delta_f = 30°$; $\delta_{a_l} = 7.85°$; $q \approx 25$ lb/sq ft.

NACA

Figs. 53,54.

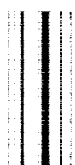

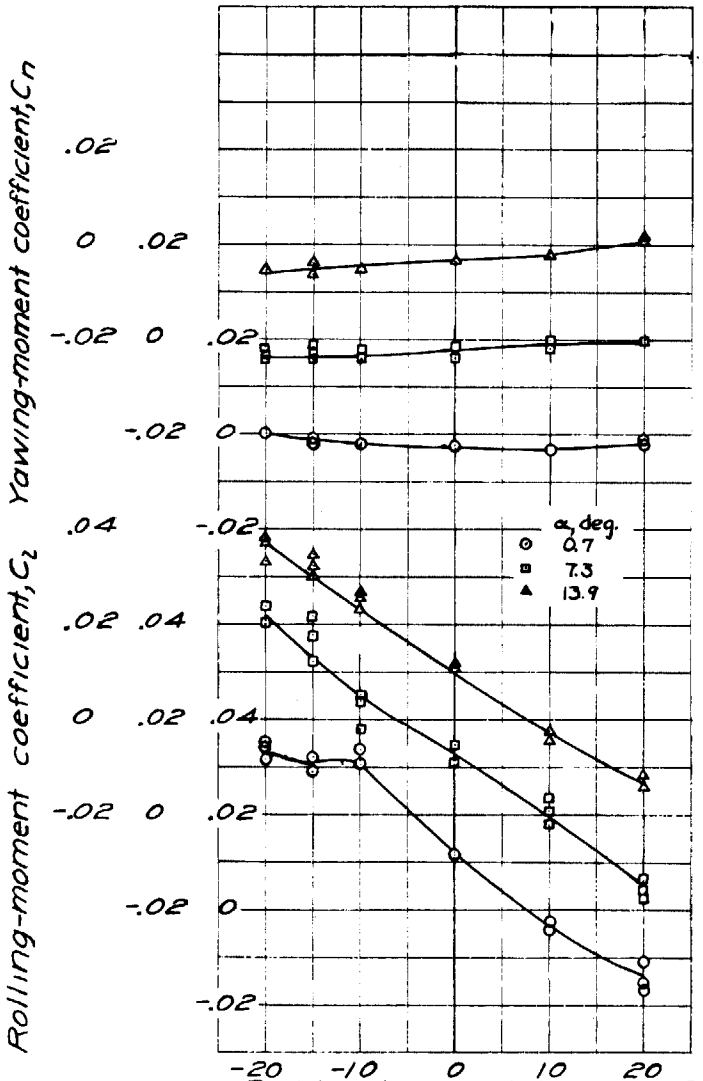

Figure 55.-Variation of rolling-moment and yawing-moment coefficients with right aileron deflection; power off; $i_t = 1.6°$; $\delta_f = 30°$; $\delta_{f_{SP}} = 0°$; $\delta_{a_l} = 7.85°$; $q \approx 25$ lb/sq ft.; $R \approx 2.6 \times 10^6$.

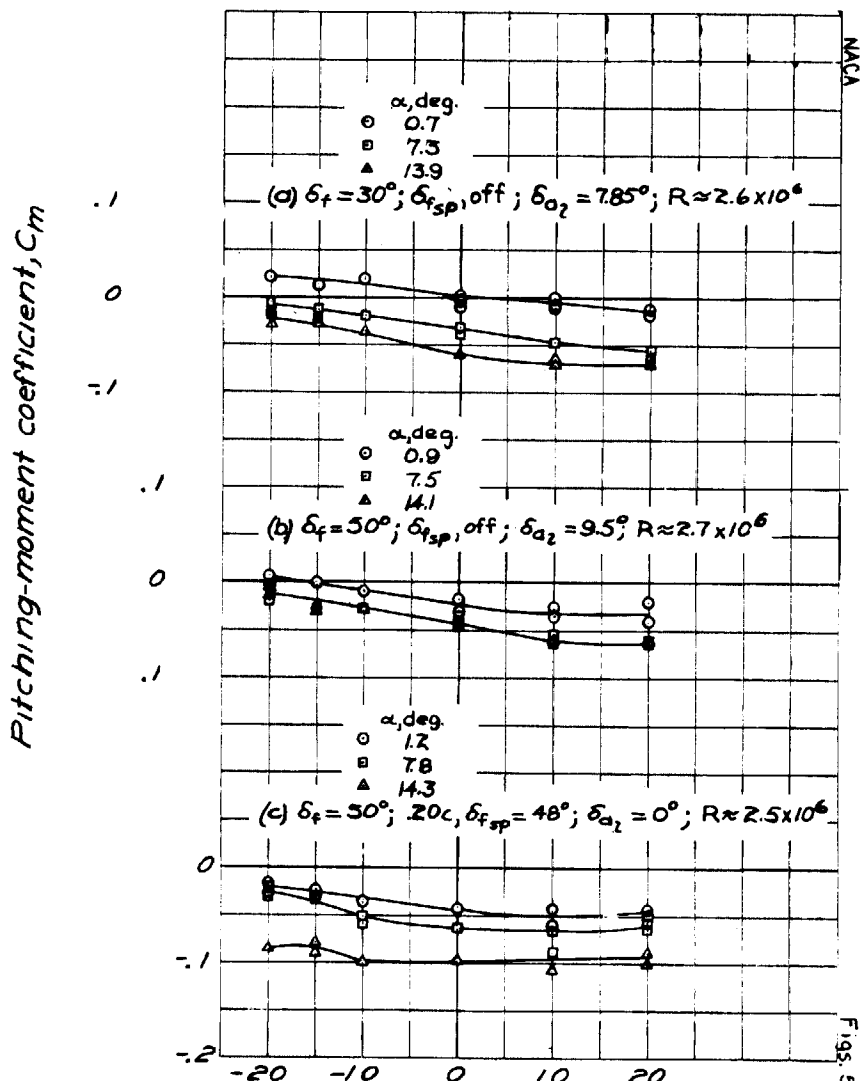

Figure 56.-Variation of pitching-moment coefficient with right aileron deflection power off; $i_t = 1.6°$; $q \approx 25$ lb/sq ft.

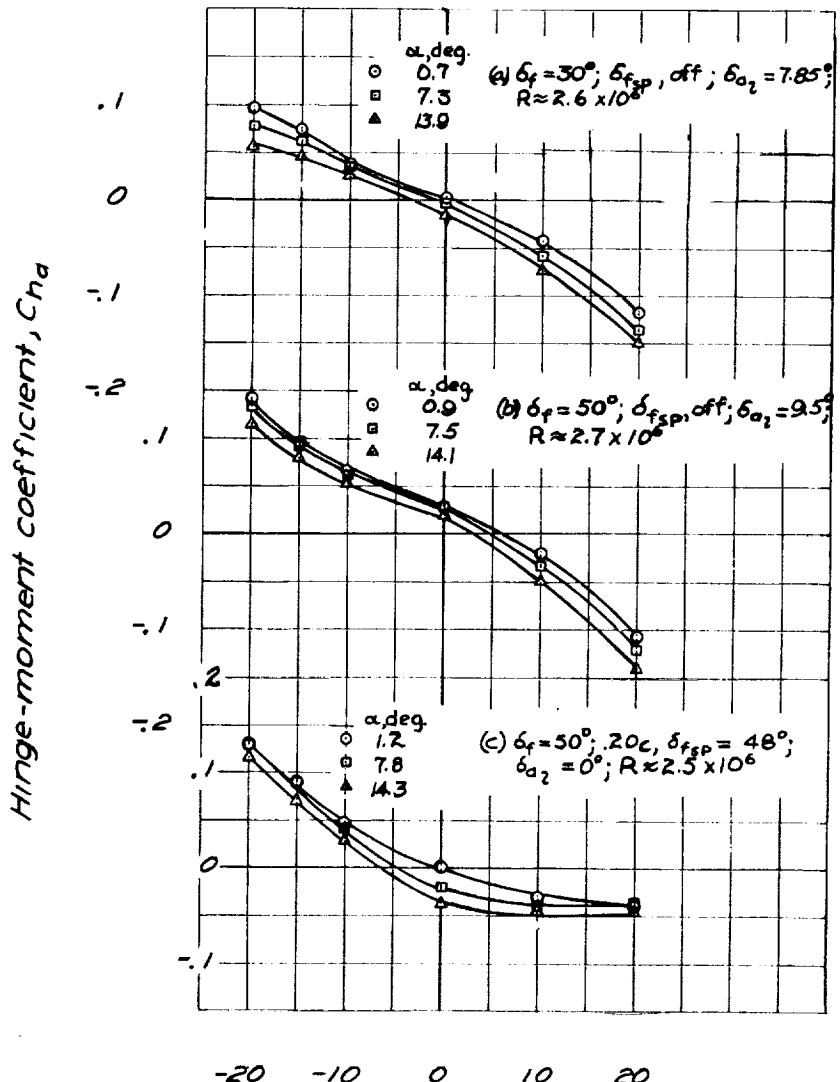

Figure 57.-Variation of hinge-moment coefficient with right aileron deflection; power off; $i_t = 1.6°$; $q = 25$ lb/sq.ft.

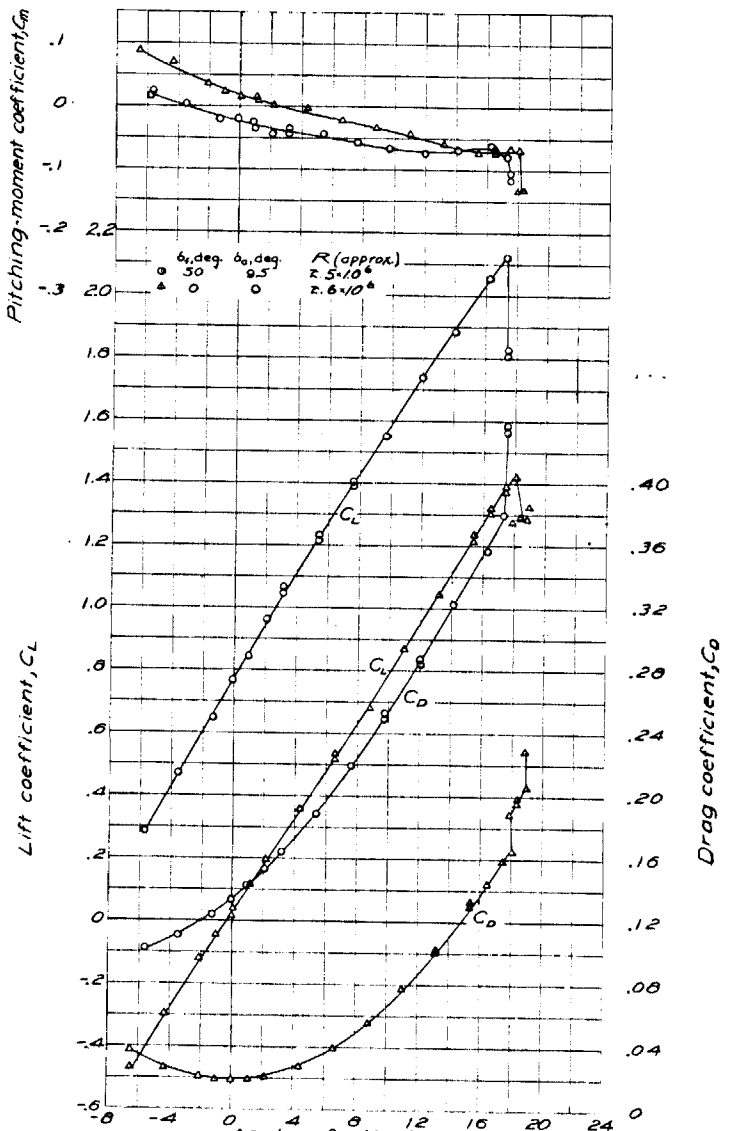

Figure 58. -Variation of lift, drag, and pitching-moment coefficients with angle of attack; droppable gas tank on; power off; $i_t = 1.6°$; $q \approx 25$ lb/sq ft.

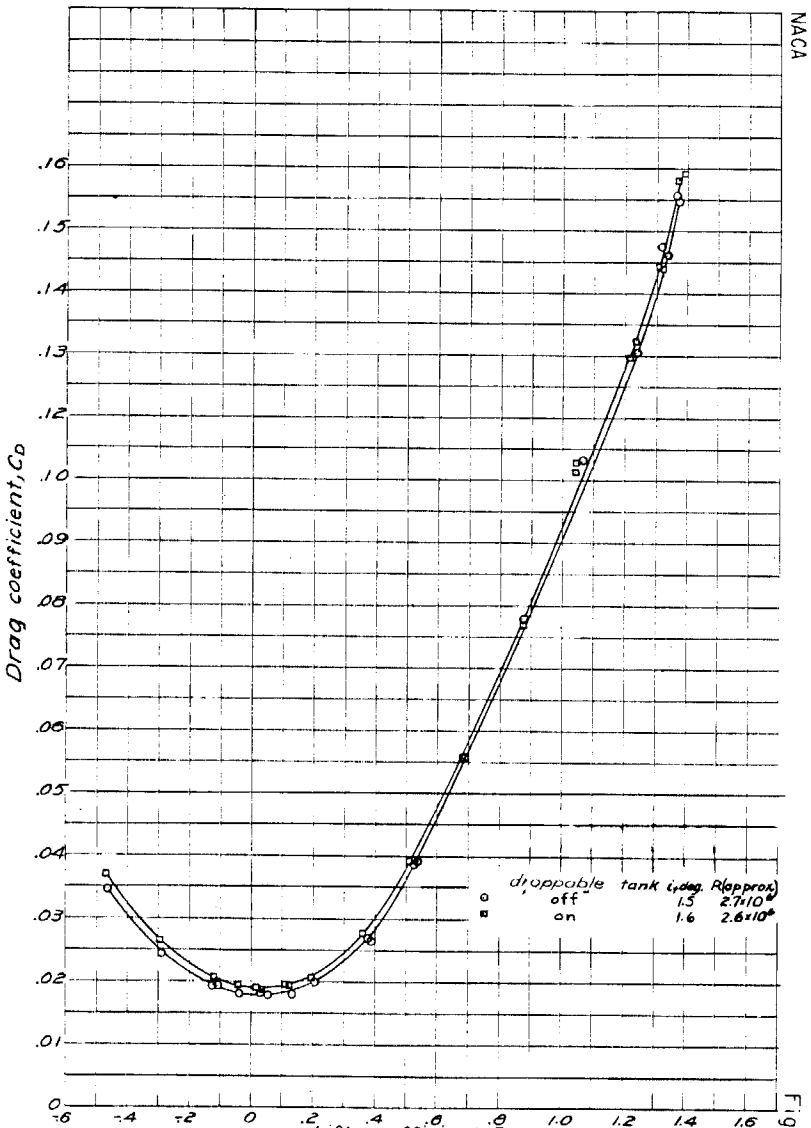

Figure 59. -Variation of lift coefficient with drag coefficient for droppable gas tank on and off; power off; $\delta_f = 0°$; $\delta_a = 0°$; $q \approx 25$ lb/sq ft.

NACA

Figs. 58,59

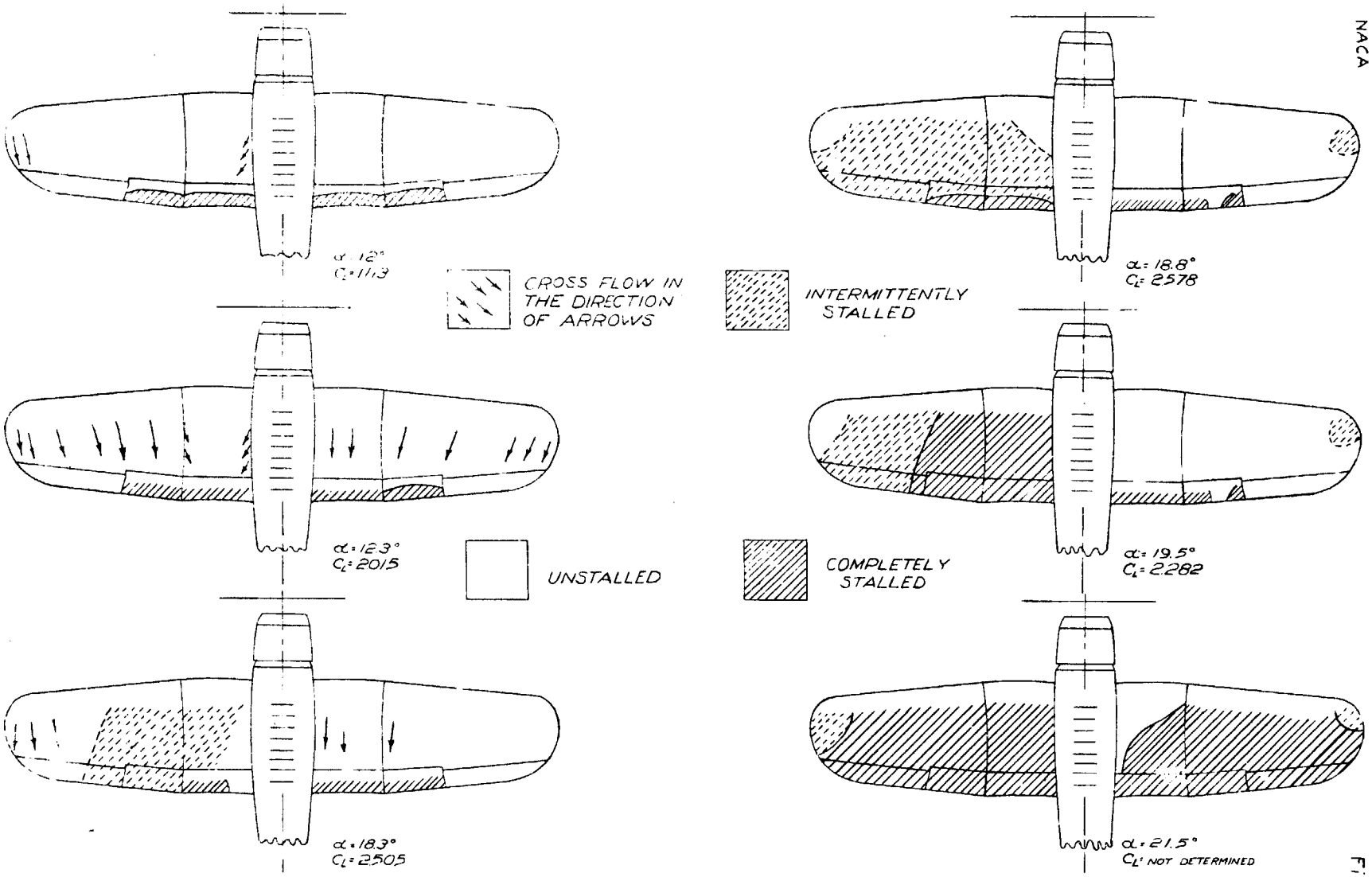

FIGURE 60.-STALL DIAGRAMS OF 1/27.5-SCALE MODEL F4U-1 AIRPLANE, ELEVATOR NOSE 5; POWER ON; i_t = 1.6°; δ_f = 50°; 0.20c $\delta_{f_{sp}}$ = 40°; δ_a = 0°; q ≈ 8.4 LB/SQ FT; R ≈ 1.6 × 10⁶.

NACA

Fig. 60

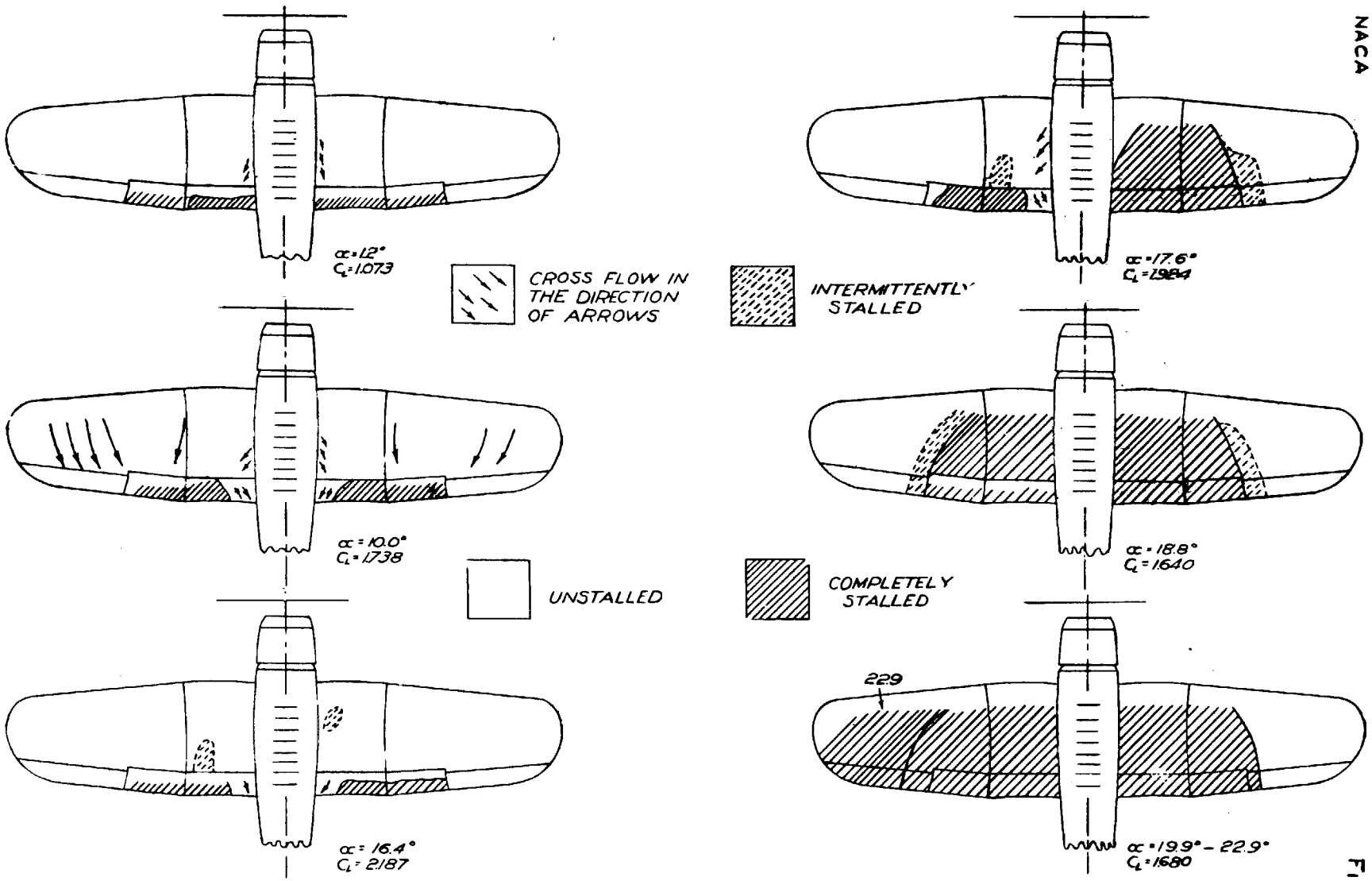

FIGURE 61 - STALL DIAGRAMS OF 1/27.5-SCALE MODEL F4U-1 AIRPLANE, ELEVATOR NOSE 5; POWER OFF i_t = 1.6°; δ_f = 50°; 0.20c δ_{tab} = 40°; δ_a = 0°; q = 25 LB/SQ. FT; R = 2.7 × 10⁶.

NACA

Fig. 61